

Predictions of damages from Atlantic tropical cyclones: a hierarchical Bayesian study on extremes

Lindsey Dietz^{1,+}, Sakshi Arya², and Snigdhanu Chatterjee^{1,*}

¹University of Minnesota, 224 Church Street SE, Minneapolis, MN 55455, USA

²Penn State University, Shortlidge Rd, State College, PA 16802, USA

*chatt019@umn.edu

+currently with the Federal Reserve Bank of Minneapolis

ABSTRACT

Bayesian hierarchical models are proposed for modeling tropical cyclone characteristics and their damage potential in the Atlantic basin. We model the joint probability distribution of tropical cyclone characteristics and their damage potential at two different temporal scales, while taking several climate indices into account. First, a predictive model for an entire season is developed that forecasts the number of cyclone events that will take place, the probability of each cyclone causing some amount of damage, and the monetized value of damages. Then, specific characteristics of individual cyclones are considered to predict the monetized value of the damage it will cause. Robustness studies are conducted and excellent prediction power is demonstrated across different data science models and evaluation techniques.

Introduction

Tropical cyclones or hurricanes are among the foremost of natural phenomena that regularly cause great harm to human communities and infrastructure¹⁻⁵. Many studies have been conducted on the physics of these storms⁶⁻¹⁰, their frequencies, intensities and potential for causing damage and the dependence of these on climatic features like teleconnections and sea-surface temperatures¹¹⁻²⁰.

However, the relationship between economic loss and a tropical cyclone's size, intensity, storm surge, rainfall and other important climatic factors, is complex and difficult to model explicitly²¹. There is a need for employing robust statistical methodologies that can leverage the observable and quantifiable properties of tropical cyclones and related climate conditions *to predict* the risks and damages that tropical cyclones can cause. In this paper, we propose a Bayesian hierarchical framework for predicting the probability that a given tropical cyclone may be damage-inflicting, and the amount of damage that it can cause. While our study is restricted to the Atlantic basin, conceptually it can be extended to any tropical cyclone basin. We provide the Bayesian predictive models at two different temporal scales. First, to aid preparation for each tropical cyclone season, we develop a predictive model that forecasts the number of cyclone events that will take place, the probability that a given cyclone will inflict damages, and the monetized value of damages. Then, to aid immediate damage mitigation interventions, we consider some physical characteristics of individual cyclone, like its minimum central pressure (minCP) and its maximum windspeed (maxWS), to predict the monetized value of the damage it will cause.

Historical changes in damages are a result of meteorological factors (climate change or as a result of human activity) and socio-economic factors (increased population in hurricane-prone areas and increased prosperity). Therefore, in order to assess the effect of climate change on hurricane trends, most studies correct for socio-economic influences by normalizing the damage data^{22,23}. A substantial number of these studies did not find a significant increase in hurricane damage since 1900 suggesting that changes in the climate have not led to noticeable increases in hurricane damage in the past^{21,22,24-28}; although some did find increases since the 1970s²⁹⁻³¹. However, the common consensus is that the Atlantic basin has substantial year-to-year and decade-to-decade variability in tropical cyclone activity levels and corresponding losses. In this light, it has been claimed²¹ that model based prediction may not be able to improve upon what is expected from long-term historical record of U.S. tropical cyclone landfalls and damages. However, our findings indicate otherwise. We address the issue of 'hurricane droughts'^{32,33} in our Bayesian framework for the seasonal scale, i.e. several years without landfall. This type of 'drought' may make a standard time series analysis of historical records and other classical statistical approaches relatively complex and inefficient, however, the proposed Bayesian framework of this paper is unaffected by such volatilities. Our model builds on and extends several data science-driven approaches for modeling tropical cyclone frequency and intensity based on natural and anthropogenic features^{11-17,19,20,34-36}.

Apart from the seasonal scale, we develop a Bayesian hierarchical framework for predicting monetary damages for each

individual tropical cyclone. For this purpose we present a hierarchical generalized extreme value probability distribution (GEV) framework that has not been studied before, coupling the maximum wind speed (maxWS), minimum central pressure (minCP) and financial damages data of tropical cyclones, while controlling for the average latitude of regions where the cyclones were recorded (details are in the Methods section).

Past studies have established the sensitivity of annual damage to individual extreme events, thus emphasizing the need for studying individual cyclone events for better estimating the risk of extreme losses and for better financial planning^{37–41}. The relationship between maxWS and minCP in tropical cyclones has been studied for several decades^{42–45}. It has been claimed that while the most accurate and reliable estimate of tropical cyclone intensity is the minCP, destructive potential is better related to maxWS⁴⁶. The frequency, intensity, and size of hurricanes are naturally also influenced by climatic factors like changes in sea surface temperature (SST), El Niño events and so on^{38,41,47–59}. It is of interest to understand the stress due to climate change on relationships between various characteristics of a cyclone, climatic factors, and the risks associated from tropical cyclones to human life and property, ecology, biodiversity and various other vulnerabilities^{43,60,61}.

In extending the above studies, the proposed framework in this paper models the joint probability distribution of (i) maxWS, (ii) minCP and (iii) damages using a Bayesian hierarchical model, with each of these conditionally modeled by a non-stationary logistic generalized extreme value distribution (GEV). The three variables maxWS, minCP and damages require joint study because data uncertainty may lead to potential changes in the joint distribution over time. Our use of extreme value probability distributions also extend several recent studies on extreme climate phenomena and related economic analyses^{16,19,45,62–66}.

In addition, we conduct thorough robustness studies with the probabilistic inferential and prediction frameworks. This is done by using, (i) several choices of prior distributions, (ii) empirical Bayesian and frequentist frameworks as alternatives to the proposed hierarchical Bayesian model, and, (iii) different mathematical optimization approaches. Details are reported in the supplementary materials. These additional studies ensure that the inferences and predictions are not sensitive to the choice of the data science model or technology used, but instead reflect what the data tells us. Proper diagnostic studies were carried out on the Markov Chain Monte Carlo (MCMC) procedures used in our studies, to ensure that the Markov chains show strong evidence of convergence, that the parameter set is sufficiently explored and the chain is well mixed. Trace, density, autocorrelation plots and various types of convergence quantifications are used for MCMC diagnostics. Our studies on the Atlantic tropical basin using different data science approaches report substantially similar inference results. Additionally, since our approach is probabilistic in nature and obtains full predictive distributions, we are able to quantify many different kinds of prediction uncertainties.

We present our findings in two parts. First, we present the results for the season-level prediction for the number of cyclones, the probability that any given cyclone will inflict some damage, and the monetized value of such damages from the hierarchical Bayesian model. The predictions from 2017 and 2019, a high cyclone activity and a low cyclone activity season respectively, are reported. Additional predictions are reported in the supplementary materials. Then the results on individual damage-causing cyclones are presented, using a hierarchical Bayesian extreme value distributional framework. We evaluate the prediction framework on cyclones of the 2016-2017 season. Discussions and comments on the obtained results are collected in the section following the results. The hierarchical Bayesian techniques used for seasonal model is presented in the first part of the Methods section, followed by the hierarchical generalized extreme value Bayesian framework for predictions of damages from individual tropical cyclones and the description of the data that we use. The supplementary materials include details about the data, technical specifications about the predictive distributional models, alternative data science and computational models, and additional predictions.

Results

Seasonal Posterior Predictive Analysis

We group the tropical cyclones into two categories based on the Saffir-Simpson hurricane wind scale⁶⁷. The first group is considered low intensity and corresponds to tropical cyclones up to category 2 in the Saffir-Simpson scale, while the second group is considered high intensity and comprises category 3-5 tropical cyclones (peak sustained winds exceeding 50 ms^{-1}). It is common in the literature to consider Saffir-Simpson Categories 3-5 Atlantic Hurricanes separately from the overall frequency, and label them major hurricanes^{21,27,28,68}. Historically, major hurricanes have accounted for about 80% of hurricane-related damages in the United States of America (USA) despite only representing 34% of USA tropical cyclone occurrences²⁸. The grouping of tropical cyclones based on whether they have low or high intensities also reflects the reality of the bimodal nature of the damage distribution depicted in Figure 1.

In each group, Gibbs sampling technique of Markov Chain Monte Carlo (MCMC) is used to estimate the posterior distribution for inference. The expected proportions of damage-inflicting cyclones were respectively estimated around 14.2% and 39% for the low and the high intensity groups. The monetary values of low and high intensity damages indicated expected value in the log-normal scale of 18.29 (with 95% credible interval = (17.63, 18.96)) and 21.12 (20.26, 21.98) respectively,

corresponding to about 87.75 million (corresponding 95% credible interval being (45.31, 171.31) million) and 1.487 billion (95% credible interval = (0.674, 3.685) billion) dollars worth of damage. Thus, on average, the U.S. should be prepared for about 1.575 billion dollars in damage each year, primarily from high-intensity tropical cyclones. Although an exact comparison is hard to make because estimates from different studies employ different methodologies and quote results based on the specific goals of their respective studies, these estimates seem to fall in the ballpark range observed in the literature^{21,25,27}.

We present the details for the 2017 and 2019 tropical cyclone seasons as illustrative examples of Bayesian seasonal predictions. The degree of tropical cyclone activity and damages in these two years considerably vary, thus providing an excellent spectrum of cases to evaluate the Bayesian predictive model. We use all available data (1960 onward) up to the prediction year and include the pre-season covariates for both low and high intensity tropical cyclones. Then our predictive model forecasts the number of cyclone events, the probability of each cyclone causing some amount of damage, and the monetized value of damages it will cause, for that season. Additional details about other years are in the supplementary materials.

We display the predictive posterior mass/density functions and actual observations for 2017 in Figure 2 and for 2019 in Figure 3. The year 2017 is known for intense tropical cyclone activity and damages³⁷, while 2019 was a much milder year with no damages. As seen in Figure 2 and 3, the actual number of cyclones, landfall frequency and damages are well within the predicted distribution for the low intensity category as well as the high intensity category. For 2019, there were no recorded damages in low intensity as well as high intensity cyclones. It can be seen from Figure 3 (lower middle plot), that observing zero landfalling high intensity cyclones had the highest chance in at around 36-37%. Also, the predictive distribution plots in Figure 3 reflect the considerable chance of no damages, with about a 22% chance for the low intensity category and 38% change for the high intensity category, respectively. It can be seen from Figure 2 and Figure 3, that the predictive model provides an excellent fit. The figures for some other years, along with additional figures where an empirical Bayesian or a fast Bayesian predictive modeling is used, are presented in the supplementary materials.

Individual Cyclones: Bayesian Predictive Analysis for 2016-17

We use the hierarchical generalized extreme value distribution (GEV) model to predict the properties of the cyclones in 2016 and 2017. Both years were active cyclone seasons⁶⁹⁻⁷², thus, are good tests for the model prediction capabilities. Since a Bayesian specification corresponds to updating the model as new data become available, we use all available data up to the prediction year and include the pre-season covariates for all cyclones starting from 1960.

There are 5 cyclones that hit continental U.S. in 2016 and 2017 with non-zero damages: Hermine and Matthew in 2016 (with normalized damage values 610 million and 11 billion, respectively), and Harvey, Irma and Nate in 2017 (with damages amounting to approximately 133 billion, 53 billion and 230 million, respectively). We assess the performance of our models by comparing where the true values for the three variables (maxWS, minCP and damages) fall on the posterior predictive distribution. For each cyclone, we find the 95% credible intervals and check whether the actual cyclone maxWS, minCP and damages are included in these intervals or not. It is observed that the true minimum central pressure values and the true maximum wind speeds were within the 95% credible interval for all the five cyclones. The credible interval could not capture the observed damage value for Harvey, but other cyclones were within the 95% interval. Missing one case out of fifteen with 95% credible intervals is not surprising: a false signalling of one in every twenty instances is expected. Another reason for the miss could be that hurricane Harvey was exceptional in the amount of damage it caused, and in such a situation, statistical risk assessment could suffer from short, incomplete and/or inaccurate past records⁷⁰.

In order to quantify exactly where the true value for each of the three variables falls on the posterior predictive distribution for the five cyclones in 2016-17, we calculate the percentile of the true value on the posterior predictive distribution. Let us call this α . Then, we calculate $\delta = 2\min\{\alpha, 1 - \alpha\}$ for each of the alpha values corresponding to each of the three variables and 5 cyclones. Note, the closer the value of δ is to 1, the closer the truth is to the posterior predictive median and if δ is closer to zero, then the truth is near the tail of the distribution. Table 2 presents the δ values and these essentially show the proposed model is an excellent predictive tool.

The 2017 hurricane season was the costliest season since records began in 1851, in large part due to the devastation wrought by major hurricanes like Harvey, Irma, and Nate³⁷. Natural disasters such as these highlight the need for quantitative estimates of the risk of such disasters. We display the posterior predictive densities for the cyclones Harvey and Irma, two of the most historically damaging cyclones, in Figure 4. As can be seen from the figure, the actual amount of minimum central pressure and maximum wind speed for both the cyclones falls well within the predicted distribution. The actual amount of damage are within the limits of the predictive distribution for both Harvey and Irma, although towards the tails for damages. For the other three tropical cyclones of 2016 and 2017, the actual values were in substantially high posterior density regions.

We conducted similar prediction analysis using a trivariate Bayesian GEV and a hierarchical Bayesian model with log-Normal damages, described in the supplementary materials, and they enforce the narrative that our results are very robust against different data science techniques used. Our predictive results also reflect that hurricanes Harvey and Irma were exceptional in

terms of the damages, at the tails but within the range of the posterior distributions. Our hierarchical Bayesian GEV model predicts that Harvey was one-in-a-thousand and Irma was one-in-twenty event in terms of damages they inflicted.

Discussion

In this paper we propose a data-driven framework for predicting the monetary value of damages caused by Atlantic tropical cyclones and storms. The framework is developed to analyze data at two time scales: for an entire season of cyclones and for each individual cyclone or storm. The seasonal model predicts storm or cyclone frequency, the probability of causing any damage and the amount of damages. The individual cyclone model predicts the minimum central pressure, maximum wind speed and the amount of damages caused. Both the models exhibit excellent predictive power as evident from Figures 2 - 4 and other figures and tables in supplementary materials. The inference results for our proposed Bayesian hierarchical models are robust, as verified by replicating the studies with alternative data science models and posterior predictive checks. The model fits are also satisfactory as seen from the diagnostics of the Markov Chain Monte Carlo procedures. Our estimates indicate that on average, the United States should prepare for approximately 1.575 billion dollars worth of damages per year at current prices, with the 2.5% and 97.5% quantile being 0.675 billion and 3.685 billion, respectively.

Our Bayesian hierarchical models can easily accommodate additional features and variables like exact location of tropical cyclone landing and degree of urbanization, monetized ecological and environmental losses⁷³ and so on. Minor computational extensions of our model can be used for variable or model selection also, for example, the exact landing spot of a tropical cyclone may not have substantial predictive value from a data science perspective. While using additional features can potentially lead to more precise predictions and narrower prediction intervals, we restrict our analysis to those features for which trustworthy and adequate data were available. The Bayesian hierarchical models proposed here may also be useful for other basins of tropical cyclone activities. However, adequate data on cyclone damages seems to be available only for the Atlantic basin currently.

Our predictive models can be useful in many ways. Forecasting tropical cyclones is a challenging task^{36,74,75}, and our proposed methodology and results can provide valuable insights here. Our models may be used by insurance and reinsurance industry⁷⁶, as well as the broader community. A data sciences framework like the one proposed in this paper can serve as a paradigm for using observable physical, chemical, biological or other observable characteristics of natural or man-made event for predicting quantifiable gains and losses resulting from the event. More generally, this paradigm can be useful for guiding the effects on different kinds of interventions, or adaptation and mitigation strategies related to the event.

Methods

Methods: Bayesian Modeling of Seasonal Cyclone Activity

We classify the cyclones for every season into two groups based on the Saffir-Simpson scale, those with low intensity (denoted by $C = 1$) and those with high intensity ($C = 2$), thus ensuring that there is a reasonable number of cyclones in each group in most years. Also, such a grouping is compatible with the bimodal distribution of damages that is evidenced from the data, see Figure 1 on the logarithm of nonzero damages. Modes on the logarithmic scales correspond approximately to damages around 24 million and 3.6 billion in 2019 dollars for the low and high intensity categories respectively.

In each season, we consider three aspects of Atlantic tropical cyclone activity. For each season/year i , these are the number of cyclones ($N_{C,i}$), the number of tropical cyclones that cause damages ($L_{C,i}$) and the valuation of the damages ($D_{C,i}$). We also consider several climatic features (X_i) that may be associated with Atlantic tropical cyclones, these include sea surface temperatures, natural phenomena like sunspots and solar magnetic disturbances, and different climate indices like the Atlantic multi-decadal oscillation index (AMO), the north Atlantic oscillation index (NAO), the southern oscillation index (SOI), the Nino3.4 anomaly index^{11,12,16,34}.

We find that the distribution of annual low intensity cyclone frequencies is over-dispersed, and hence use a negative binomial parameterization for it, as in (1). In each group, the frequency of cyclones that inflict economic damages is captured using a binomial distribution, conditional on the frequency of cyclones in each group for a given year, see (2). The actual valuation of cyclone damages is modeled using a mixture distribution with a mass at zero and a lognormal distribution, as in (3). The precise mathematical details of the model are given below, with a detailed description in the supplementary materials. The

notation $[X]$ for a random variate X denotes its distribution.

$$[N_{1,i}|X_i, r, p_i, \beta_1] \sim \text{NegBinom}(r, p_i) \quad (1)$$

$$p_i = \frac{r}{r + \lambda(x_i)}$$

$$\log(\lambda(x_i)) = x_i \beta_1; \beta_1 \in \mathbb{R}^{q_1}$$

$$[L_{1,i}|N_{1,i} = n_{1,i}, X_i, \phi, \beta_1, \theta_1] \sim \text{Binomial}(n_{1,i}, \theta_1) \quad (2)$$

$$[D_{1,i}|L_{1,i}, N_{1,i} = n_{1,i}, X_i, \phi, \beta_1, \theta_1, \mu_1, \sigma_1] \sim (1 - (1 - \theta_1)^{n_{1,i}}) * \text{Lognormal}(\mu_1, \sigma_1) + (1 - \theta_1)^{n_{1,i}} * 0 \quad (3)$$

$$[\beta_1] \sim \mathcal{N}(0_{q_1}, 10^5 I_{q_1}), \quad (4)$$

with priors, $[\theta_1] \sim \text{Beta}(1, 1)$, $[\mu_1] \sim \mathcal{N}(0, 10^5)$, $\frac{1}{\sigma_1^2} \sim \text{Gamma}(1, 1)$ and $[r] \sim \text{Unif}(0, 70)$, respectively.

The hierarchical specification for the high intensity cyclones is similar to that of low intensity except that the cyclone frequencies are modeled as Poisson distribution with mean parameter, $\gamma(\mathbf{X}) = \mathbf{X}\beta_2$, as in (5). The model specification is given below and the details for the model are in the supplementary materials (section A.1).

$$[N_{2,i}|X_i, \beta_2] \sim \text{Poisson}(\lambda(x_i)) \quad (5)$$

$$\log(\lambda(x_i)) = x_i \beta_2; \beta_2 \in \mathbb{R}^{q_2}$$

$$[L_{2,i}|N_{2,i}, X_i, \beta_2, \theta_2] \sim \text{Binomial}(n_{2,i}, \theta_2) \quad (6)$$

$$[D_{2,i}|L_{2,i}, N_{2,i}, X_i, \beta_2, \theta_2, \mu_2, \sigma_2] \sim (1 - (1 - \theta_2)^{n_{2,i}}) * \text{Lognormal}(\mu_2, \sigma_2) + (1 - \theta_2)^{n_{2,i}} * 0 \quad (7)$$

$$[\beta_2] \sim \mathcal{N}_2(0_{q_2}, 10^5 I_{q_2}) \quad (8)$$

with priors, $[\theta_2] \sim \text{Beta}(1, 1)$, $[\mu_2] \sim \mathcal{N}(0, 10^5)$ and $[1/\sigma_2^2] \sim \text{Gamma}(1, 1)$, respectively.

To ensure the results and inference we obtain from the data are not sensitive to modeling assumptions, we repeated the analysis using several alternative statistical models and data science formalism. In the supplementary materials we report an empirical Bayesian modeling approach and a different computational approach that uses data cloning. The results of all these alternative data modeling approaches are also in the supplementary materials, and are all substantially identical, confirming the robustness of the results to modeling framework.

Methods: Bayesian Modeling of Individual Cyclones

We consider a hierarchical Bayesian model to jointly model a tropical cyclone's minimum central pressure (minCP), maximum windspeed (maxWS) and the monetary value of the damages that the cyclone caused. Let Z_1 represents $\log(\text{minCP})$, Z_2 is for standardized average latitude, X_1 represents $\log(\text{maxWS})$ and X_2 is for $\log(\text{damages})$. We use the notation GEV for the *generalized extreme value distribution*⁷⁷. We consider the following hierarchical GEV model:

$$[Z_1|Z_2] \sim \text{GEV}(\mu_{z_1}(Z_2), \sigma_{z_1}, \xi_{z_1}) \quad (9)$$

$$[X_1|(Z_1, Z_2)] \sim \text{GEV}(\mu_{x_1}(Z_1, Z_2), \sigma_{x_1}, \xi_{x_1}) \quad (10)$$

$$[X_2|(X_1, Z_1, Z_2)] \sim \text{GEV}(\mu_{x_2}(X_1, Z_1, Z_2), \sigma_{x_2}, \xi_{x_2}), \quad (11)$$

where the hierarchy is in the location parameters $\mu_{z_1}(Z_2) = \alpha_0 + \alpha_1 Z_2$, $\mu_{x_1}(Z_1, Z_2) = \beta_0 + \beta_1 Z_1 + \beta_2 Z_2$ and $\mu_{x_2}(X_1, Z_1, Z_2) = \gamma_0 + \gamma_1 X_1 + \gamma_2 Z_1 + \gamma_3 Z_2$. The joint density can then be written as,

$$f(Z_1, X_1, X_2|Z_2, \theta) = \frac{1}{\sigma_{x_2}} (t(x_2))^{\xi_{x_2}+1} \exp(-t(x_2)) \frac{1}{\sigma_{x_1}} (t(x_1))^{\xi_{x_1}+1} \exp(-t(X_1)) \frac{1}{\sigma_{z_1}} (t(z_1))^{\xi_{z_1}+1} \exp(-t(Z_1)), \text{ where,}$$

$$t(x) = \begin{cases} (1 + \xi(\frac{x-\mu}{\sigma}))^{-1/\xi} & \xi \neq 0 \\ \exp(-\frac{x-\mu}{\sigma}) & \xi = 0. \end{cases}$$

Our choice of priors are essentially non-informative with variances chosen to ensure proper coverage of the sample space and reasonably good acceptance rates in the Metropolis-Hastings algorithm. These are $\alpha_0, \alpha_1, \beta_0, \beta_1, \beta_2 \stackrel{iid}{\sim} \mathcal{N}(0, 10^2)$,

$\gamma_0, \gamma_1, \gamma_2, \gamma_3 \stackrel{iid}{\sim} N(0, 10^3)$, $\sigma_{z_1}, \sigma_{x_1} \stackrel{iid}{\sim} IG(\alpha = 1, \beta = 1)$, $\sigma_{x_2} \sim IG(\alpha = 2, \beta = 3)$, $\xi_{z_1} \sim \text{Unif}(-1, 1)$, $\xi_{x_1}, \xi_{x_2} \stackrel{iid}{\sim} \text{Unif}(-0.5, 0.5)$. The notations N, IG and Unif respectively stand for the Normal/Gaussian distribution, the inverse Gamma distribution and the Uniform distribution.

In Table 1, we report the frequentist maximum likelihood estimates (MLE) and their standard errors, as well as Bayes estimators and their standard deviations corresponding to (9), (10) and (11). For the Bayesian computations, a Markov Chain Monte Carlo (MCMC) algorithm is implemented for $N = 10^6$ size and the step-sizes are chosen to achieve about 20% acceptance rate.

The coefficient of average latitude (α_1) in modeling the location parameter for minCP is statistically significant. Similarly, the effect of minCP (β_1) in modeling location parameter for maxWS seems to be significant and the effect of maxWS (γ_1) on log(damages) seems also to be significant. The scale and shape parameter estimates are significant across models, with a negative estimate for the shape parameters signifying reverse Weibull distributions for the marginals of each of the three variables, log(minCP), log(maxWS) and log(damages), respectively. The diagnostics of the MCMC algorithm show that mixing and other properties of the Markov chain are all fully satisfactory.

Data Description

The National Hurricane Center (NHC) maintains the North Atlantic-basin hurricane database (HURDAT2, or Best Track), containing six-hourly information on the location, maximum winds, central pressure, and (beginning in 2004) size of all known tropical cyclones and subtropical cyclones since 1851⁷⁸. We use the data from the Atlantic tropical cyclone basin from 1960 up to 2019 in HURDAT2. Data prior to 1960 is not used in this study owing to possible inaccuracies. We define the maximum category a cyclone achieves by applying the Saffir-Simpson scale to the highest maximum wind speed¹ over the cyclone's lifetime. Tropical storms are included with tropical cyclones due to several damage events attributed to these less powerful cyclones. Monetized damage estimates for all tropical cyclones since 1900 have been compiled²⁵, and updated by the ICAT catastrophe insurance company <http://www.icatdamageestimator.com/>. The data is normalized to 2019 dollars to reflect changes in inflation, wealth, and population in the cyclone area²⁵.

We use the Atlantic Multidecadal Oscillation (AMO), the Southern Oscillation Index (SOI), the North Atlantic Oscillation (NAO), Niño 3.4 anomaly series, sea surface temperature SST and sunspot activity SSN as covariates. The Atlantic Multidecadal Oscillation (AMO) is an ongoing series of long-duration changes in the sea surface temperature of the North Atlantic Ocean, with cool and warm phases that may last for 20-40 years at a time. It is the ten-year running mean of detrended Atlantic SST Anomalies north of the equator. Data⁷⁹ are retrieved from the National Oceanic and Atmospheric Administration (NOAA), Earth System Research Laboratories (ESRL) <http://www.esrl.noaa.gov/psd/data/timeseries/AMO/>. The relationship between AMO and hurricane frequency has been studied previously, with some attributing the increase in hurricane activity to increases in AMO^{34,80-83}.

The Southern Oscillation Index (SOI) is defined as the normalized sea-level pressure difference between Tahiti and Darwin. Negative values of the SOI indicate an El Niño event. Monthly SOI values are obtained from National Centers for Environmental Prediction's (NCEP) Climate Prediction Center (CPC) <ftp://ftp.cpc.ncep.noaa.gov/wd52dg/data/indices/soi>. Annual averages of SOI over the months of August-October are used as indicators of shear upon North Atlantic hurricanes^{84,85}.

The North Atlantic Oscillation (NAO) is characterized by fluctuations in sea level pressure differences. Strong positive phases of the NAO tend to be associated with above-average temperatures in the eastern United States and thus, provide a conducive environment for tropical cyclone development. Index values for the NAO are calculated as the difference in sea level pressure between Gibraltar and a station over southwest Iceland and are collected from Physical Sciences Laboratory (PSL), NOAA <https://psl.noaa.gov/data/correlation/nao.data>.

The Niño 3.4 anomaly series is collected from NCEP CPC <http://www.cpc.ncep.noaa.gov/data/indices/ersst5.nino.mth.91-20.ascii>. This series is an average of the SST from 5°S-5°N by 170°W-120°W with the 1951-2000 mean removed. Other Niño indices exist but are highly correlated with Niño 3.4, and are less commonly used in literature.

Sea-surface temperatures (SST) are an important component for tropical intensification. Higher SST, all else being constant, is believed to provide a more conducive environment for tropical cyclone development^{18,86}. Atlantic SST averages gridded values over the region from 10-25°N by 80°W-20°W. Raw (unsmoothed and not detrended) monthly SST values are obtained via the NOAA PSL <https://psl.noaa.gov/data/gridded/tables/sst.html>. This is version 5 of the data known as ERSST and was constructed using the most recently available ICOADS SST data⁸⁷.

Sunspots are magnetic disturbances (SSN) of the sun surface having both dark and brighter regions. Variations in solar activity are monitored by sunspots. These are visible disturbances on the photosphere of the sun. The brighter regions increase the intensity of the ultraviolet emissions. Increased sunspot numbers correspond to more magnetic disturbances, which some

¹Maximum wind speed is defined as maximum wind speed value over a 1-minute period

studies predict leads to reduction in potential intensity of hurricanes³⁵. SSN are obtained from World Data Center-Sunspot Index and Long-term Solar Observations at the Royal Observatory of Belgium <http://www.sidc.be/silso/datafiles>.

We use the monthly time series available for each covariate. Previous works¹⁹ suggest an average of the May and June values of the SOI, NAO, and Atlantic SST anomalies for prediction. We operate under this same premise for AMO and the Niño 3.4 anomaly. However, with SSN we use the average of the monthly average sunspots for July to June of the predicting year, i.e. for 2019, we average July 2018 to June 2019 monthly values.

References

1. Dietz, L. R. *Advanced Statistical Modeling Constructs for Climate Extremes*. Ph.D. thesis, University of Minnesota (2016).
2. Elsner, J. B., Elsner, G. J. B. & Kara, A. B. *Hurricanes of the North Atlantic: Climate and society* (Oxford University Press on Demand, 1999).
3. Rappaport, E. N. Loss of life in the united states associated with recent atlantic tropical cyclones. *Bull. Am. Meteorol. Soc.* **81**, 2065–2074 (2000).
4. Field, C. B. *et al.* Ipcc, 2012: Summary for policymakers: Managing the risks of extreme events and disasters to advance climate change adaptation. In *Planning for Climate Change*, 111–128 (Routledge, 2018).
5. Wuebbles, D. J., Fahey, D. W. & Hibbard, K. A. *Climate science special report: fourth national climate assessment, volume I* (U. S. Global Change Research Program, 2017).
6. Emanuel, K. Tropical cyclones. *Annu. review earth planetary sciences* **31**, 75–104 (2003).
7. Zhou, W., Held, I. M. & Garner, S. T. Parameter study of tropical cyclones in rotating radiative–convective equilibrium with column physics and resolution of a 25-km gcm. *J. Atmospheric Sci.* **71**, 1058–1069 (2014).
8. Liang, J. & Wu, L. Sudden track changes of tropical cyclones in monsoon gyres: Full-physics, idealized numerical experiments. *J. Atmospheric Sci.* **72**, 1307–1322 (2015).
9. Vidale, P. L. *et al.* Impact of stochastic physics and model resolution on the simulation of tropical cyclones in climate gcms. *J. Clim.* **34**, 4315–4341 (2021).
10. Tamizi, A., Alves, J.-H. & Young, I. R. The physics of ocean wave evolution within tropical cyclones. *J. Phys. Oceanogr.* **51**, 2373–2388 (2021).
11. Elsner, J. B. Tracking Hurricanes. *Bull. Am. Meteorol. Soc.* **84**, 353–356 (2003).
12. Elsner, J. B., Bossak, B. H. & Niu, X. Secular Changes to the ENSO-U.S. Hurricane Relationship. *Geophys. Res. Lett.* **28**, 4123–4126 (2001).
13. Elsner, J. B. & Jagger, T. H. A Hierarchical Bayesian Approach to Seasonal Hurricane Modeling. *J. Clim.* **17**, 2813–2827 (2004).
14. Elsner, J. B. & Jagger, T. H. Comparison of Hindcasts Anticipating the 2004 Florida Hurricane Season. *Weather. Forecast.* **21**, 182–192 (2005).
15. Elsner, J. B. & Jagger, T. H. Prediction Models for Annual U.S. Hurricane Counts. *J. Clim.* **19**, 2935–2951 (2006).
16. Jagger, T. H. & Elsner, J. B. A consensus model for seasonal hurricane prediction. *J. Clim.* **23**, 6090–6099 (2010).
17. Villarini, G., Vecchi, G. A. & Smith, J. A. Modeling the Dependence of Tropical Storm Counts in the North Atlantic Basin on Climate Indices. *Am. Meteorol. Soc.* **138**, 2681–2705 (2010).
18. Dailey, P. S., Zuba, G., Ljung, G., Dima, I. M. & Guin, J. On the Relationship between North Atlantic Sea Surface Temperatures and U.S. Hurricane Landfall Risk. *J. Appl. Meteorol. Climatol.* **48**, 111–129 (2009).
19. Jagger, T. H., Elsner, J. B. & Saunders, M. A. Forecasting U.S. Insured Hurricane Losses. In Diaz, H. F. & Murnane, R. J. (eds.) *Climate Extremes and Society*, 189–208 (Cambridge University Press, 2008).
20. Jagger, T. H., Elsner, J. B. & Burch, R. K. Climate and solar signals in property damage losses from hurricanes affecting the United States. *Nat. Hazards* **58**, 541–557 (2010).
21. Pielke, R. A. United States Hurricane Landfalls and Damages: Can One- to Five-Year Predictions Beat Climatology? *Environ. Hazards* **8**, 187–200 (2009).
22. Pielke, R. A. & Landsea, C. W. Normalized hurricane damages in the united states: 1925–95. *Weather. forecasting* **13**, 621–631 (1998).

23. Grinsted, A., Ditlevsen, P. & Christensen, J. H. Normalized us hurricane damage estimates using area of total destruction, 1900– 2018. *Proc. Natl. Acad. Sci.* **116**, 23942–23946 (2019).
24. Schmidt, S., Kemfert, C. & Hölpe, P. Tropical cyclone losses in the usa and the impact of climate change—a trend analysis based on data from a new approach to adjusting storm losses. *Environ. Impact Assess. Rev.* **29**, 359–369 (2009).
25. Pielke, R. A., Gratz, J., Landsea, C. W., Collins, D. & Musulin, M. A. S. R. Normalized Hurricane Damage in the United States: 1900–2005. *Nat. Hazards* **9**, 29–42 (2008).
26. Bouwer, L. M. & Wouter Botzen, W. How sensitive are us hurricane damages to climate? comment on a paper by wd nordhaus. *Clim. Chang. Econ.* **2**, 1–7 (2011).
27. Weinkle, J. *et al.* Normalized hurricane damage in the continental united states 1900–2017. *Nat. Sustain.* **1**, 808–813 (2018).
28. Vecchi, G. A., Landsea, C., Zhang, W., Villarini, G. & Knutson, T. Changes in atlantic major hurricane frequency since the late-19th century. *Nat. communications* **12**, 1–9 (2021).
29. Miller, S., Muir-Wood, R. & Boissonnade, A. An exploration of trends in normalized weather-related catastrophe losses. *Clim. extremes society* **12**, 225–247 (2008).
30. Nordhaus, W. D. The economics of hurricanes and implications of global warming. *Clim. Chang. Econ.* **1**, 1–20 (2010).
31. Knutson, T. R. *et al.* Climate change is probably increasing the intensity of tropical cyclones. In *Critical issues in climate change science* (ScienceBrief Review, 2021).
32. Hall, T. & Hereid, K. The Frequency and Duration of U.S. Hurricane Droughts. *Geophys. Res. Lett.* **42**, 3482–3485 (2015).
33. Hall, T. & Hereid, K. The frequency and duration of us hurricane droughts. *Geophys. Res. Lett.* **42**, 3482–3485 (2015).
34. Loehle, C. & Staehling, E. Hurricane trend detection. *Nat. Hazards* **104**, 1345–1357 (2020).
35. Hodges, R. E., Jagger, T. H. & Elsner, J. B. The sun-hurricane connection: Diagnosing the solar impacts on hurricane frequency over the north atlantic basin using a space–time model. *Nat. hazards* **73**, 1063–1084 (2014).
36. Vecchi, G. A. *et al.* On the seasonal forecasting of regional tropical cyclone activity. *J. Clim.* **27**, 7994–8016 (2014).
37. Halverson, J. B. The costliest hurricane season in us history. *Weatherwise* **71**, 20–27 (2018).
38. Mudd, L., Wang, Y., Letchford, C. & Rosowsky, D. Assessing climate change impact on the us east coast hurricane hazard: temperature, frequency, and track. *Nat. Hazards Rev.* **15**, 04014001 (2014).
39. Landsea, C. W., Pielke, R. A., Mestas-Nunez, A. M. & Knaff, J. A. Atlantic basin hurricanes: Indices of climatic changes. *Clim. change* **42**, 89–129 (1999).
40. Blake, E. S., Landsea, C. W. & Gibney, E. J. The Deadliest, Costliest, and Most Intense United States Tropical Cyclones From 1851 to 2010 (and Other Frequently Requested Hurricane Facts). Tech. Rep., NOAA (2011).
41. Ye, M., Wu, J., Liu, W., He, X. & Wang, C. Dependence of tropical cyclone damage on maximum wind speed and socioeconomic factors. *Environ. Res. Lett.* **15**, 094061 (2020).
42. Atkinson, G. D. & Holliday, C. R. Tropical cyclone minimum sea level pressure/maximum sustained wind relationship for the western north pacific. *Mon. Weather. Rev.* **105**, 421–427 (1977).
43. Wang, Y. & Wu, C. C. Current understanding of tropical cyclone structure and intensity changes – a review. *Meteorol. Atmospheric Phys.* **87**, 257–278 (2004).
44. Kieu, C. Q., Chen, H. & Zhang, D.-L. An Examination of the Pressure–Wind Relationship for Intense Tropical Cyclones. *Weather. Forecast.* **25**, 895–907 (2010).
45. Chavas, D. R., Reed, K. A. & Knaff, J. A. Physical understanding of the tropical cyclone wind–pressure relationship. *Nat. communications* **8**, 1–11 (2017).
46. Knaff, J. A. & Zehr, R. M. Reexamination of Tropical Cyclone Wind–Pressure Relationships. *Weather. Forecast.* **22**, 71–88 (2007).
47. Goldenberg, S. B. & Shapiro, L. J. Physical mechanisms for the association of el niño and west african rainfall with atlantic major hurricane activity. *J. Clim.* **9**, 1169–1187 (1996).
48. Zhao, M. & Held, I. M. An analysis of the effect of global warming on the intensity of atlantic hurricanes using a gcm with statistical refinement. *J. Clim.* **23**, 6382–6393 (2010).

49. DeMaria, M., Sampson, C. R., Knaff, J. A. & Musgrave, K. D. Is tropical cyclone intensity guidance improving? *Bull. Am. Meteorol. Soc.* **95**, 387–398 (2014).
50. Villarini, G., Vecchi, G. A. & Smith, J. A. Modeling the dependence of tropical storm counts in the north atlantic basin on climate indices. *Mon. Weather. Rev.* **138**, 2681–2705 (2010).
51. Patricola, C. M., Chang, P. & Saravanan, R. Degree of simulated suppression of atlantic tropical cyclones modulated by flavour of el niño. *Nat. Geosci.* **9**, 155–160 (2016).
52. Huang, Z., Rosowsky, D. V. & Sparks, P. R. Long-term hurricane risk assessment and expected damage to residential structures. *Reliab. engineering & system safety* **74**, 239–249 (2001).
53. Wang, C., Li, Q., Pang, L., Zou, A. & Zhang, L. Hurricane damage assessment for residential construction considering the non-stationarity in hurricane intensity and frequency. *Acta Oceanol. Sinica* **35**, 110–118 (2016).
54. Pant, S. & Cha, E. J. Wind and rainfall loss assessment for residential buildings under climate-dependent hurricane scenarios. *Struct. Infrastructure Eng.* **15**, 771–782 (2019).
55. Emmanuel, K. A. Increasing Destructiveness of Tropical Cyclones Over the Past 30 years. *Nature* **436**, 686–688 (2005).
56. Senkbeil, J. C. & Sheridan, S. C. A postlandfall hurricane classification system for the united states. *J. Coast. Res.* **22**, 1025–1034 (2006).
57. Lin, N., Smith, J. A., Villarini, G., Marchok, T. P. & Baeck, M. L. Modeling extreme rainfall, winds, and surge from hurricane isabel (2003). *Weather. forecasting* **25**, 1342–1361 (2010).
58. Rezapour, M. & Baldock, T. E. Classification of hurricane hazards: The importance of rainfall. *Weather. Forecast.* **29**, 1319–1331 (2014).
59. Wang, C. Sensitivity of tropical cyclone damage costs to integrated wind profile. *J. Ocean. Eng. Sci.* (2021).
60. Maclay, K. S., DeMaria, M. & Haar, T. H. V. Tropical Cyclone Inner-Core Kinetic Energy Evolution. *Mon. Weather. Rev.* **136**, 4882–4898 (2008).
61. Mei, W., Pasquero, C. & Primeau, F. The Effect of Translation Speed upon the Intensity of Tropical Cyclones over the Tropical Ocean. *Geophys. Res. Lett.* **39**, 1–6 (2012).
62. Economou, T., Stephenson, D. B. & Ferro, C. A. Spatio-temporal modelling of extreme storms. *The Annals Appl. Stat.* **8**, 2223–2246 (2014).
63. Waylen, P. R. Modeling the effects of tropical cyclones on flooding in the santa fe river basin, florida. *GeoJournal* **23**, 361–373 (1991).
64. Chikobvu, D. & Chifurira, R. Modelling of extreme minimum rainfall using generalised extreme value distribution for zimbabwe. *South Afr. J. Sci.* **111**, 01–08 (2015).
65. Hernández Ayala, J. J., Keellings, D., Waylen, P. R. & Matyas, C. J. Extreme floods and their relationship with tropical cyclones in puerto rico. *Hydrol. Sci. J.* **62**, 2103–2119 (2017).
66. Miniussi, A., Villarini, G. & Marani, M. Analyses through the metastatistical extreme value distribution identify contributions of tropical cyclones to rainfall extremes in the eastern united states. *Geophys. Res. Lett.* **47** (2020).
67. Taylor, H. T., Ward, B., Willis, M. & Zaleski, W. The saffir-simpson hurricane wind scale. *Atmospheric Adm. Washington, DC, USA* (2010).
68. Goldenberg, S. B., Landsea, C. W., Mestas-Nuñez, A. M. & Gray, W. M. The recent increase in atlantic hurricane activity: Causes and implications. *Science* **293**, 474–479 (2001).
69. Murakami, H., Levin, E., Delworth, T., Gudgel, R. & Hsu, P.-C. Dominant effect of relative tropical atlantic warming on major hurricane occurrence. *Science* **362**, 794–799 (2018).
70. Emanuel, K. Assessing the present and future probability of hurricane harvey’s rainfall. *Proc. Natl. Acad. Sci.* **114**, 12681–12684 (2017).
71. Pilkington, S. F. & Mahmoud, H. N. Real-time application of the multihazard hurricane impact level model for the atlantic basin. *Front. built environment* **3**, 67 (2017).
72. Thomas, A. *et al.* Influence of storm timing and forward speed on tides and storm surge during hurricane matthew. *Ocean. Model.* **137**, 1–19 (2019).
73. Pruitt, J. N., Little, A. G., Majumdar, S. J., Schoener, T. W. & Fisher, D. N. Call-to-action: A global consortium for tropical cyclone ecology. *Trends ecology & evolution* **34**, 588–590 (2019).

74. Camp, J. *et al.* Seasonal forecasting of tropical storms using the met office glosea5 seasonal forecast system. *Q. J. Royal Meteorol. Soc.* **141**, 2206–2219 (2015).
75. Vecchi, G. A. & Villarini, G. Next season's hurricanes. *Science* **343**, 618–619 (2014).
76. Dlugolecki, A. F. Climate change and the insurance industry. *The Geneva Pap. on Risk Insur. Pract.* **25**, 582–601 (2000).
77. De Haan, L., Ferreira, A. & Ferreira, A. *Extreme value theory: an introduction*, vol. 21 (Springer, 2006).
78. Landsea, C. W. & Franklin, J. L. Atlantic Hurricane Database Uncertainty and Presentation of a New Database Format. *Mon. Weather. Rev.* **141**, 3576–3592 (2013).
79. Enfield, D. B., Mestas-Nunez, A. M. & Trimble, P. J. The Atlantic Multidecadal Oscillation and its relationship to rainfall and river flows in the continental U.S. *Geophys. Res. Lett.* **28**, 2077–2080 (2001).
80. Trenberth, K. E. & Shea, D. J. Atlantic hurricanes and natural variability in 2005. *Geophys. research letters* **33** (2006).
81. Zhang, R. & Delworth, T. L. Impact of atlantic multidecadal oscillations on india/sahel rainfall and atlantic hurricanes. *Geophys. research letters* **33** (2006).
82. Li, S., Wang, Y., Gao, Y. *et al.* A review of the researches on the atlantic multidecadal oscillation (amo) and its climate influence. *Transactions Atmospheric Sci.* **32**, 458–465 (2009).
83. Alexander, M. A., Kilbourne, K. H. & Nye, J. A. Climate variability during warm and cold phases of the atlantic multidecadal oscillation (amo) 1871–2008. *J. Mar. Syst.* **133**, 14–26 (2014).
84. Elsner, J. B., Kossin, J. P. & Jagger, T. H. The increasing intensity of the strongest tropical cyclones. *Nature* **455**, 92–95 (2008).
85. Hodges, R. E. & Elsner, J. B. The spatial pattern of the sun-hurricane connection across the north atlantic. *Int. Sch. Res. Notices* **2012** (2012).
86. Fraza, E. & Elsner, J. B. A climatological study of the effect of sea-surface temperature on north atlantic hurricane intensification. *Phys. Geogr.* **36**, 395–407 (2015).
87. Smith, T. M., Reynolds, R. W., Peterson, T. C. & Lawrimore, J. Improvements to NOAA's Historical Merged Land–Ocean Surface Temperature Analysis. *J. Clim.* **21**, 2283–2296 (2008).

Acknowledgements (not compulsory)

This research is partially supported by the US National Science Foundation (NSF) under grants # 1737918, # 1939916 and # 1939956.

Author contributions statement

SC conceived the research problem and planned the data analysis experiments, LD collected the data and conducted the first round of analysis, SA updated the data and conducted a further round of analysis. All authors contributed towards drafting the manuscript, and reviewed the manuscript.

Additional information

Authors declare no competing interests.

	MLE	Std. Error	Bayes estimator	Posterior SD
α_0	-0.1919	0.0930	-0.1111	0.0857
α_1	-0.2623	0.0608	-0.2707	0.0497
σ_{z_1}	1.0395	0.0744	0.7730	0.0299
ξ_{z_1}	-0.5859	0.0499	-0.4320	0.0413
β_0	4.3691	0.0128	4.2234	0.0310
β_1	0.3430	0.0151	0.3534	0.0279
β_2	-0.0449	0.0128	-0.0421	0.0310
σ_{x_1}	0.1429	0.0088	0.3554	0.0170
ξ_{x_1}	-0.3521	0.0444	-0.4876	0.0127
γ_0	19.5008	0.2033	19.2674	0.1732
γ_1	0.9391	0.5735	1.0667	0.3850
γ_2	0.5070	0.5535	0.4374	0.3717
γ_3	-0.1918	0.2068	-0.1398	0.1395
σ_{x_2}	2.2626	0.1394	1.5835	0.0536
ξ_{x_2}	-0.3275	0.0373	-0.1971	0.0253

Table 1. Maximum likelihood estimates with standard errors, Bayes estimates (posterior means, posterior standard deviations) from models (9), (10), (11) from the fully hierarchical Bayesian extreme value distribution (GEV) model

Hurricanes	minCP	maxWS	Damage
Hermine (2016)	0.8549	0.5408	0.3648
Matthew (2016)	0.3659	0.2008	0.2044
Harvey (2017)	0.2909	0.3541	0.0012
Irma (2017)	0.1974	0.1631	0.0546
Nate (2017)	0.9325	0.0514	0.5099

Table 2. The δ values for each damaging tropical cyclone of 2016 and 2017, using the hierarchical GEV model. A δ value close to 1 reflects the truth to be close to the median of the posterior predictive distribution, and close to 0 reflects the truth lying in the tails of the distribution.

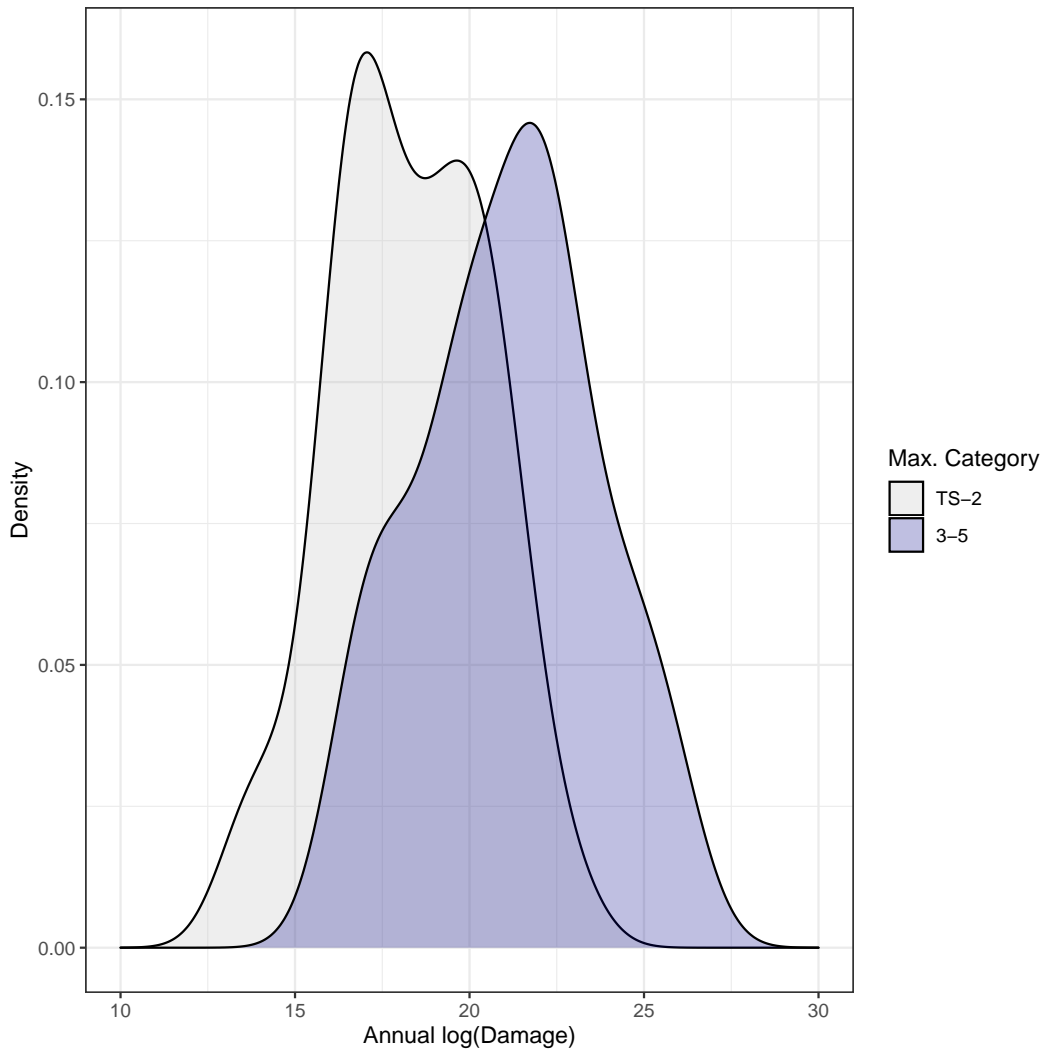


Figure 1. Estimated Densities of Annual Log Damage in US dollars for Cyclones in Low and High Intensity Categories.

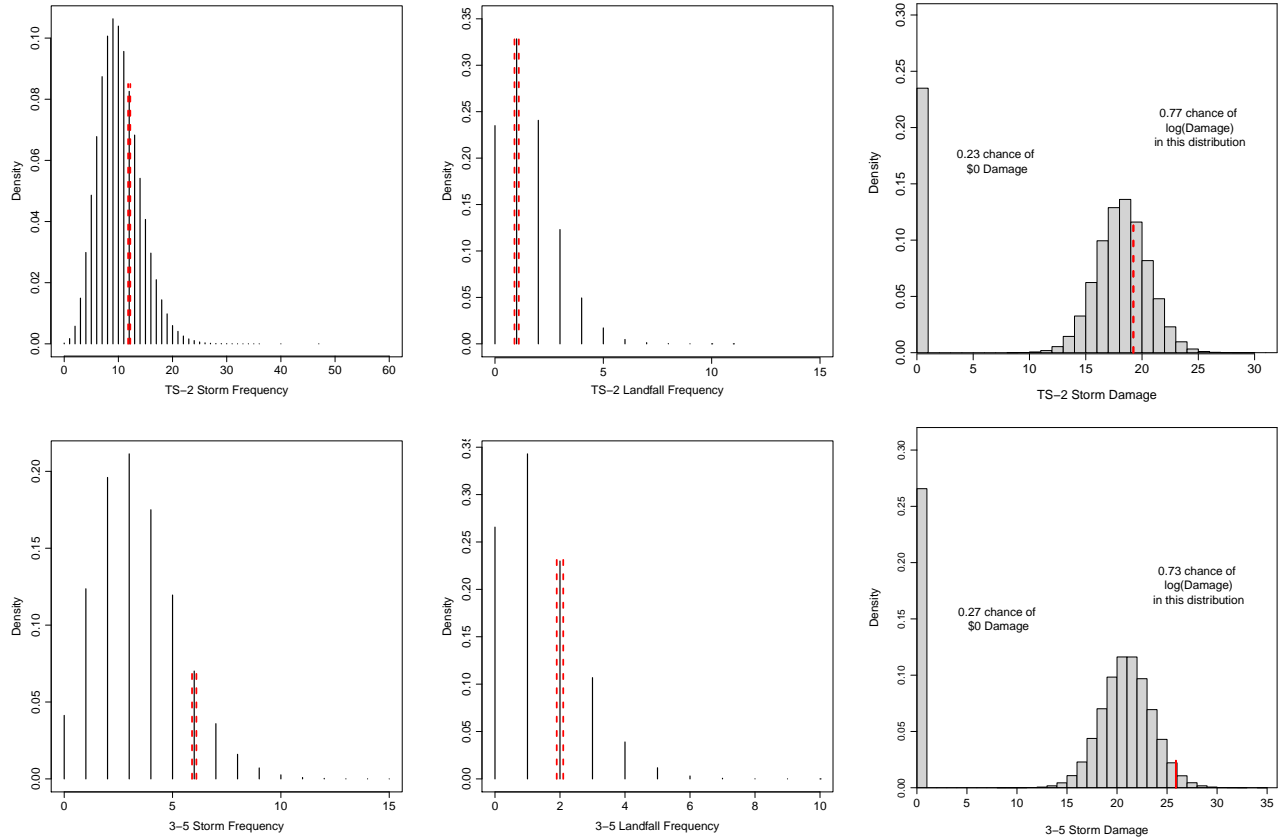


Figure 2. Posterior Predictive Distributions for 2017 tropical cyclones. The upper row is for the low intensity case, the bottom row is for the high intensity case. The left column displays the probability mass function of the Bayesian predictive distribution for frequency of cyclones, the middle column is the predicted probability mass function of whether a tropical cyclone may cause damage, and the right column is the predictive density for damages. The actual observed values are displayed with red dashed lines.

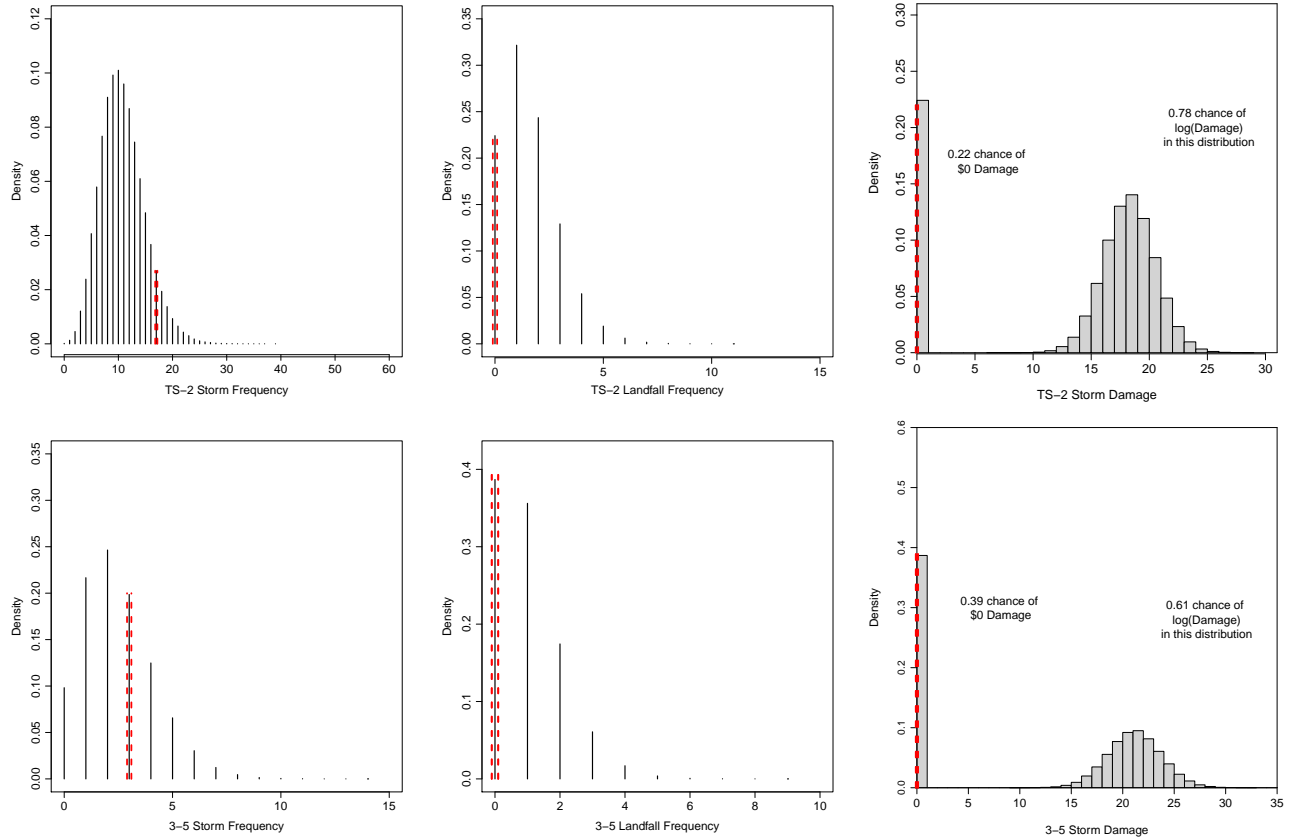


Figure 3. Posterior Predictive Distributions for 2019 tropical cyclones. The upper row is for the low intensity case, the bottom row is for the high intensity case. The left column displays the probability mass function of the Bayesian predictive distribution for frequency of cyclones, the middle column is the predicted probability mass function of a cyclone to cause damage, and the right column is the predictive density for damages. The actual observed values are displayed with red dashed lines.

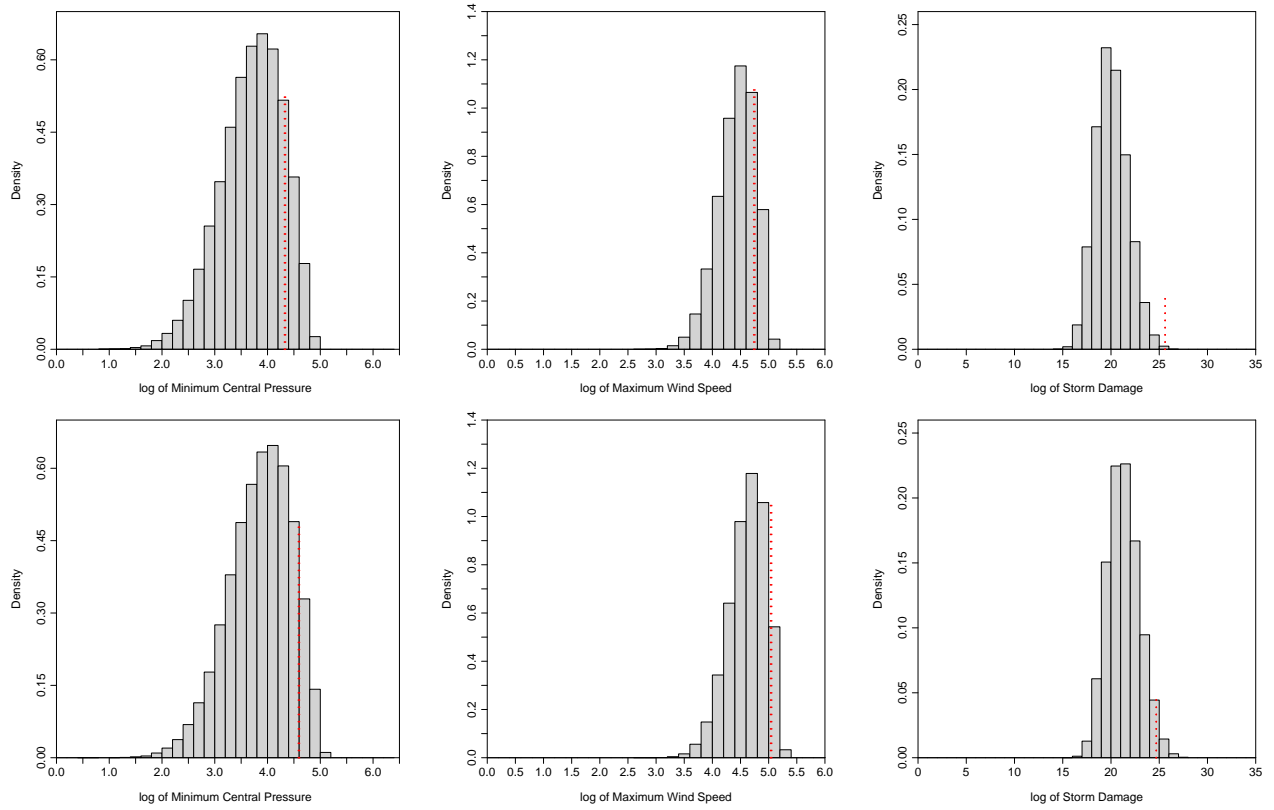


Figure 4. Posterior Predictive Distributions for minCP, maxWS and damages of tropical cyclones Harvey and Irma, based on the hierarchical Bayesian GEV model. The actual values for the cyclones are displayed with red dashed lines.

A Supplementary: Model Details, and Additional Data Analysis

A.1 Bayesian Model For Seasonal Analysis: Details

Recall that the cyclones are in two groups, low and high intensity, and we use the generic notation C for a group. Let occurrence frequency of group C in year i be represented by $N_{C,i}$, and let the frequency of damage-causing cyclones in group C in year i be represented by $L_{C,i}$. Finally, let damages in year i be represented as $D_{C,i}$. Let the corresponding vector collections of all years for these variables be \mathbf{N}_C , \mathbf{L}_C , and \mathbf{D}_C . For a given year, i , define annual covariates as X_i .

The distribution of annual low intensity cyclone frequencies is modeled as a negative binomial distribution. In (12), we parameterize the negative binomial density for observation i with p_i and r . The latter is the (over)dispersion parameter, which in the Poisson distribution equals 1 (no overdispersion). The former is referred to as the success parameter, and for observation i is defined as $p_i = r/(r + \lambda_i)$, where $\log \lambda_i = \sum_j \beta_j X_{ij}$.

Frequency of damage-inflicting tropical cyclones, \mathbf{L}_1 , is modeled using a binomial distribution with parameter θ_1 in (2) based on the elements in the vector of annual frequencies, \mathbf{N}_1 . Finally, damages, \mathbf{D}_1 , are modeled in (3) using a mixture distribution with a mass at 0 and nonzero damage modeled by a lognormal distribution with parameter (μ_1, σ_1) .

Priors are specified independently and employ normal distributions for β_1 , and μ_1 as in (15) and (17), respectively. The distribution of θ_1 is specified in (16) using a Beta distribution and σ_1 in (18) using an inverse transformation to a Gamma distribution. In addition, we use a uniform prior that puts an upper bound of 70 for r , as in (19). This is not restrictive as the negative binomial tends to the Poisson as $r \rightarrow \infty$.

The hierarchical specification for the high intensity cyclones is similar to that of low intensity save for the cyclone occurrence distribution. Cyclone occurrence in (21) utilizes a Poisson distribution with mean parameter, $\gamma(\mathbf{X}) = \mathbf{X}\beta_2$. As in the low intensity case, the frequency of damage-inflicting cyclones, \mathbf{L}_2 , is modeled using a binomial distribution with parameter θ_2 in (22) based on the vector of annual frequencies, \mathbf{N}_2 . Finally, damages, \mathbf{D}_2 , are modeled in (23) using a mixture distribution with a mass at 0 and nonzero damage modeled by a lognormal distribution with parameter (μ_2, σ_2) . Priors are specified independently and employ normal distributions for β_2 and μ_2 as in (24) and (26), respectively. The distribution of β_2 is specified with independent components. Similar to the low intensity case, θ_2 is specified using a Beta distribution in (25), and σ_2 is specified in (27) using an inverse transformation to a Gamma distribution.

Below, we specify the precise model that we used in this paper. We use the notations $\mathbf{0}_{q_1}$ for a vector of 0s of length q and I_q for an identity matrix of size $q \times q$ where q depends on the number of covariates in the model being fit.

Low Intensity Cyclone Fully Bayesian Specification:

$$[N_{1,i}|X_i, r, p_i, \beta_1] \sim \text{NegBinom}(r, p_i) \quad (12)$$

$$p_i = \frac{r}{r + \lambda(x_i)}$$

$$\log(\lambda(x_i)) = x_i \beta_1; \beta_1 \in \mathbb{R}^{q_1}$$

$$[L_{1,i}|N_{1,i}, X_i, \phi, \beta_1, \theta_1] \sim \text{Binomial}(n_{1,i}, \theta_1) \quad (13)$$

$$[D_{1,i}|L_{1,i}, N_{1,i}, X_i, \phi, \beta_1, \theta_1, \mu_1, \sigma_1] \sim$$

$$(1 - (1 - \theta_1)^{n_{i1}}) * \text{Lognormal}(\mu_1, \sigma_1) + (1 - \theta_1)^{n_{i1}} * 0 \quad (14)$$

$$[\beta_1] \sim \mathcal{N}(\mathbf{0}_{q_1}, 10^5 I_{q_1}) \quad (15)$$

$$[\theta_1] \sim \text{Beta}(1, 1) \quad (16)$$

$$[\mu_1] \sim \mathcal{N}(0, 10^5) \quad (17)$$

$$\left[\frac{1}{\sigma_1^2} \right] \sim \text{Gamma}(1, 1) \quad (18)$$

$$[r] \sim \text{Unif}(0, 70) \quad (19)$$

High Intensity Cyclone Fully Bayesian Specification:

$$[N_{2,i}|X_i, \beta_2] \sim \text{Poisson}(\lambda(x_i)) \quad (20)$$

$$\log(\lambda(x_i)) = x_i \beta_2; \beta_2 \in \mathbb{R}^{q_2} \quad (21)$$

$$[L_{2,i}|N_{2,i}, X_i, \beta_2, \theta_2] \sim \text{Binomial}(n_{2,i}, \theta_2) \quad (22)$$

$$[D_{2,i}|L_{2,i}, N_{2,i}, X_i, \beta_2, \theta_2, \mu_2, \sigma_2] \sim$$

$$(1 - (1 - \theta_2)^{n_{i2}}) * \text{Lognormal}(\mu_2, \sigma_2) + (1 - \theta_2)^{n_{i2}} * 0 \quad (23)$$

$$[\beta_2] \sim \mathcal{N}_2(\mathbf{0}_{q_2}, 10^5 I_{q_2}) \quad (24)$$

$$[\theta_2] \sim \text{Beta}(1, 1) \quad (25)$$

$$[\mu_2] \sim \mathcal{N}(0, 10^5) \quad (26)$$

$$\left[\frac{1}{\sigma_2^2} \right] \sim \text{Gamma}(1, 1) \quad (27)$$

A.2 Additional Analysis: Empirical Bayesian Modeling Of Seasonal Data

To corroborate the full hierarchical Bayesian model presented in Section 5, we carried out multiple studies. One is an empirical Bayesian study, where we used the maximum likelihood estimators to inform the prior. The technical details are given below. As can be seen from Tables 3 and 4, the results from empirical Bayes are very close to those obtained using the hierarchical Bayesian model.

Low Intensity Cyclone Bayesian Specification (EB):

$$[N_{1,i}|X_i, r, p_i, \boldsymbol{\beta}_1] \sim \text{NegBinom}(r, p_i) \quad (28)$$

$$p_i = \frac{r}{r + \lambda(x_i)}$$

$$\log(\lambda(x_i)) = x_i \boldsymbol{\beta}_1; \boldsymbol{\beta}_1 \in \mathbb{R}^{q_1}$$

$$[L_{1,i}|N_{1,i}, X_i, \phi, \boldsymbol{\beta}_1, \theta_1] \sim \text{Binomial}(n_{1,i}, \theta_1) \quad (29)$$

$$[D_{1,i}|L_{1,i}, N_{1,i}, X_i, \phi, \boldsymbol{\beta}_1, \theta_1, \mu_1, \sigma_1] \sim (1 - (1 - \theta_1)^{n_{i1}}) * \text{Lognormal}(\mu_1, \sigma_1) + (1 - \theta_1)^{n_{i1}} * 0 \quad (30)$$

$$[\boldsymbol{\beta}_1] \sim \mathcal{N}((\hat{\beta}_{11}, \dots, \hat{\beta}_{1q_1}), 10^4 I_{q_1}) \quad (31)$$

$$[\log(\phi)] \sim \mathcal{N}(\log(\hat{\phi}), 1) \quad (32)$$

$$[\theta_1] \sim \text{Beta}(\alpha(\hat{p}_1), \beta(\hat{p}_1)) \quad (33)$$

$$[\mu_1] \sim \mathcal{N}(\bar{x}_1, 10^4) \quad (34)$$

$$[r] \sim \text{Unif}(0, 70) \quad (35)$$

$$\left[\frac{1}{\sigma_1^2} \right] \sim \text{Gamma}(v_{11}(\hat{s}_1), v_{12}(\hat{s}_1)) \quad (36)$$

High Intensity Cyclone Bayesian Specification (EB):

$$[N_{2,i}|X_i, \boldsymbol{\beta}_2] \sim \text{Poisson}(\lambda(x_i)) \quad (37)$$

$$\log(\lambda(x_i)) = x_i \boldsymbol{\beta}_2; \boldsymbol{\beta}_2 \in \mathbb{R}^{q_2}$$

$$[L_{2,i}|N_{2,i}, X_i, \boldsymbol{\beta}_2, \theta_2] \sim \text{Binomial}(n_{2,i}, \theta_2) \quad (38)$$

$$[D_{2,i}|L_{2,i}, N_{2,i}, X_i, \boldsymbol{\beta}_2, \theta_2, \mu_2, \sigma_2] \sim (1 - (1 - \theta_2)^{n_{i2}}) * \text{Lognormal}(\mu_2, \sigma_2) + (1 - \theta_2)^{n_{i2}} * 0 \quad (39)$$

$$[\boldsymbol{\beta}_2] \sim \mathcal{N}_2([\hat{\beta}_{21}, \dots, \hat{\beta}_{2q_2}]^T, 10^4 I_{q_2}) \quad (40)$$

$$[\theta_2] \sim \text{Beta}(\alpha(\hat{p}_2), \beta(\hat{p}_2)) \quad (41)$$

$$[\mu_2] \sim \mathcal{N}(\bar{x}_2, 10^4) \quad (42)$$

$$\left[\frac{1}{\sigma_2^2} \right] \sim \text{Gamma}(v_{21}(\hat{s}_2), v_{22}(\hat{s}_2)) \quad (43)$$

A.3 Additional Analysis: Data Clone Computations On Seasonal Data

In addition to the hierarchical Bayes and empirical Bayes computations, we also used `dclone`⁸⁸ method to analyze the data, and provide further support and justification about the robustness of our findings.

Data cloning was implemented using 1, 2, and 5 clones. We report the estimates of the the 5 clone chain. Each run consisted of running 3 chains of length 100,000 with adaptation on the first 100 iterations. The Markov Chain Monte Carlo (MCMC) procedure with Gibbs sampling was also implemented using 3 chains, each with 100,000 iterations. The first 100 iterations of each chain were discarded.

We report some comparison results across different statistical methodologies in Tables 3 and 4. Here, we either used all the covariates, or used a select few depending on a statistical model selection criterion (in these cases, both Akaike and Bayesian model selection suggested the same model, where a few covariates are dropped). We compare the empirical Bayesian approach with the full hierarchical Bayesian approach for both these choices. Model fitting was done either by MCMC, or by adapting the non-Bayesian data cloning approach. The tables report the posterior mean and standard deviation for the different parameter values, for these various combinations. Both tables demonstrate that there is little difference between the results from different techniques, and that we have excellent robustness against a choice of statistical methodology. Additional robustness studies were also conducted. We have used the hierarchical Bayesian approach with all covariates as the main approach for the results reported in the paper.

A.4 Seasonal Prediction Details

We utilize the Bayesian specification to get an estimate of the posterior predictive distribution. Let the distributional specification of the data $\mathbf{Y} = [\mathbf{N}, \mathbf{L}, \mathbf{D}]$ given parameters $\gamma = [\beta, \theta, \mu, \sigma, \phi]$ be $p(y|\gamma)$. Also, let the posterior distribution of γ given the data \mathbf{Y} and the hyperparameter α be $p(\gamma|y, \alpha)$. Then, the posterior predictive distribution for a new observation, $\tilde{\mathbf{Y}}$ is

$$p(\tilde{y}|y, \alpha) = \int p(\tilde{y}|\gamma)p(\gamma|y, \alpha)d\gamma \quad (44)$$

This is obtained computationally as follows:

1. Let $\{\hat{\gamma}_i; i = 1, \dots, T\}$ be the MCMC set of posterior samples.
2. Using each of these posterior estimates, we sample a new y (N, L, D) given $\hat{\gamma}_i$ using the covariates for test data. We call this new y as $y_{\text{pred}}^{(i)}$.
3. Plot a histogram (density) using all the predicted y 's, i.e., $\{y_{\text{pred}}^{(i)}; i = 1, \dots, T\}$.

Since the above steps involve massive computations, we also explored two simpler approaches, outlined below:

- **Empirical Bayesian prediction:**

1. Obtain the posterior sample mean from the hierarchical Bayesian model fit in Section 5, call them $\hat{\gamma}_{HB}$.
2. Sample 10^5 times from model specification $p(\tilde{y}|\hat{\gamma}_{HB})$ for each of the response variables, i.e., frequency of cyclones, frequency of damage-inflicting cyclones and value of damages. This provides a single realization of the posterior predictive distribution.

- **Fast computation Bayesian prediction:**

1. Let $\{\hat{\gamma}_i; i = 1, \dots, T\}$ be the MCMC set of posterior samples. Note, T is the number of posterior samples obtained in the MCMC output.
2. Using each of these posterior estimates, we sample y (N, L, D), $S = 1000$ times using the covariates for test data. We call this new y as $y_{\text{pred}_j}^{(i)}$.
- 3a. Now estimate the density $p(\tilde{y}|\hat{\gamma}_i)$ using a kernel density estimate:

$$\hat{p}(\tilde{y}|\hat{\gamma}_i) = \frac{1}{Sh} \sum_{j=1}^S K \left(\frac{\tilde{y} - y_{\text{pred}_j}^{(i)}}{h} \right)$$

- 3b. The predictive posterior distribution can then be estimated as:

$$\hat{p}(\tilde{y}|y, \alpha) = \frac{\sum_{i=1}^T \hat{p}(\tilde{y}|\hat{\gamma}_i)}{T}$$

4. Sample from the predictive posterior distribution $\hat{p}(\tilde{y}|y, \alpha)$.

Predictive inference results for the above two methods are given in Section B, along with the fully hierarchical Bayesian prediction model given in Section 2. It can be seen that the results look very similar across the three methods of predictive posterior inference.

B Appendix: Interpretation Of Posterior Predictive Densities (Seasonal Analysis)

We present a detailed discussion, and additional figures, for the Bayesian predictive analysis.

We discuss the results in detail for 2016-2019 below, to illustrate how the probability density or mass functions depicted in these figures reflect the data. In each analysis, we use the hierarchical Bayesian model, described in Section 2, the empirical Bayesian prediction and the fast computation Bayesian prediction, both described in Section A.4.

B.1 2016 Posterior Predictive Bayesian Analysis

The results are presented in Figure 5 for low intensity cyclones and in Figure 6 for high intensity cyclones. The results for 2016 indicate the model matches well with the data. The three posterior predictive methods provide similar output except that the second method has slightly more variability and provides a smoother density curve because of the averaging. As seen in Figure 5 (three figures in first (left) panel/column), the actual number of cyclones was well within the predicted distribution for the low intensity category and had at least 30% of the probability higher than the observed value. Similarly, in Figure 6 (first column), high intensity cyclone occurrence, although falling at the start of the right tail end, was within the limits of the predictive distribution.

For low intensity tropical cyclones, the predictive distribution in Figure 5(three figures in the second (middle) column) indicated that a given cyclone would inflict damages in 2016, was given approximately a 31-32% chance in each of the three versions of posterior predictive distributions. The corresponding figures for high intensity damage-inflicting cyclones in Figure 6(second column) are around 31-32%. There were \$550 million in low intensity damages, thus, Figure 5(three figures in the third (right) column) reflect the actual amount of damage for 2016 falls well within the predicted distribution for the low intensity category with non-zero damages. There were a \$ 1 billion in high intensity damages in 2016. The high intensity damages in Figure 6(third column) indicate that the true value of damage falls well within the posterior predictive range for the non-zero values. Although, there is a greater chance of no (\$0) damages (about 55%) and the log of damage incurred in 2016 had about an 8% chance of occurrence.

B.2 2017 Posterior Predictive Bayesian Analysis

Similar to 2016, results for 2017 indicate the model matches well with the observations. Again, the two posterior predictive methods provide similar output with the second method showing more variability and a smoother density curve.

As seen in Figure 7(three figures in first (left) column), the actual number of cyclones was well within the predicted distribution for the low intensity category and had at least 30% of the probability higher than the observed value. Similarly, in Figure 8(first column), high intensity cyclone occurrence, although falling at the start of the right tail end, was within the limits of the predictive distribution.

From Figure 7(three figures in the second (middle) column) indicated that in 2017, a low intensity cyclone has the probability of about 33-34% for causing damages in each of the three versions of posterior predictive distributions. Observing two high intensity damage-inflicting cyclones as in 2017 had approximately a 23-24% chance in Figure 8(middle column). There were \$225 million in low intensity damages, thus, Figure 7(three figures in the third (right) column) reflect the chance of the corresponding damage appropriately and the log of the actual amount of damage for 2017 falls well within the predicted distribution for the low intensity category with non-zero damages. The high intensity damages in Figure 8(third column) indicate the log of damage incurred in 2017 (\$175 billion) although slightly in the right end of the distribution with about an 2-3% chance of occurrence.

B.3 2018 Posterior Predictive Bayesian Analysis

Similar to the previous two years results for 2018 indicate the model matches well with the observations. Again, the three posterior predictive methods provide similar output with the second method showing a smoother density curve for damages because of the averaging. A major difference with the previous two years here is that the true damage value for 2018 (marked in red) is \$0.

The results for 2018 indicate the model matches well with the data. As seen in Figure 9(three figures in first (left) column), the actual number of cyclones was well within the predicted distributions. Similarly, in Figure 10(first column), high intensity cyclone occurrence was also within the limits of the predictive distribution. The observed value of 2 cyclones accounted for nearly 24% of the samples.

For low intensity tropical cyclones, the predictive distribution in Figure 9(three figures in second column) indicated that observing no damage-inflicting cyclone, as in 2018, was given approximately a 22-23% chance in each of the three versions of posterior predictive distributions. Similarly, observing no high intensity damage-inflicting cyclone as in 2018 had the probability in Figure 10(middle column) at around 36-37%. There were \$0 in low intensity as well as high intensity damages, thus, Figure 9(three figures in last (right) column), and Figure 11 (third column) reflect the chance of no damages appropriately and the actual amount of damage for 2018 falls well within the predicted distribution with about a 23% chance for the low intensity category and 37% change for the high intensity category, respectively, for zero damages.

B.4 2019 Posterior Predictive Bayesian Analysis

Similar to the previous three years results for 2019 indicate the model matches well with the observations. Again, the three posterior predictive methods provide similar output with the second method showing a smoother density curve for damages because of the averaging. Note that the true damage value for 2019 (marked in red) is also \$0.

The results for 2019 indicate the model matches well with the data, as seen in Figure 11(three figures in first (left) column) and in Figure 12(left column).

For low intensity tropical cyclones, the predictive distribution in Figure 11(three figures in second (middle) column) indicated that observing no damage-inflicting cyclone, as in 2019, was given approximately a 22-23% chance in each of the three versions of posterior predictive distributions. Similarly, observing zero high intensity damage-inflicting cyclone had the probability in Figure 12(middle column) at around 36-37%. There were \$0 in low intensity as well as high intensity damages, thus, Figure 11(three figures in last (right) column), and Figure 12 (last column) reflect the chance of no damages appropriately and the actual amount of damage for 2018 falls well within the predicted distribution with about a 22% chance for the low intensity category and 38% change for the high intensity category, respectively, for zero damages.

C Appendix: Additional Analysis Of Individual Cyclones Data

C.1 Individuation Cyclones: Trivariate Extreme Value Model

Here, we model $\mathbf{Y} = [\mathbf{maxWS}, \mathbf{minCP}, \mathbf{Damage}]$ using a trivariate extreme values distribution (GEV) model. Let X_1 denote the logarithm of maxWS, X_2 denote logarithm of damages and Z_1 denote the logarithm of minCP. We also add non-stationarity in the location parameters to fully utilize all information, including the average latitudes, namely, Z_2 . We consider the following hierarchy in modeling the location parameters,

$$\begin{aligned}\mu_{z_1}(Z_2) &= \alpha_0 + \alpha_1 Z_2 \\ \mu_{x_1}(Z_1, Z_2) &= \beta_0 + \beta_1 Z_1 + \beta_2 Z_2 \\ \mu_{x_2}(X_1, Z_1, Z_2) &= \gamma_0 + \gamma_1 X_1 + \gamma_2 Z_1 + \gamma_3 Z_2.\end{aligned}$$

The location and scale parameters have subscripts indicating the variable they represent. The joint distribution of a logistic dependence model⁸⁹ for three variables (Z_1, X_1, X_2) is given by,

$$G(z_1, x_1, x_2) = \exp(-(t(z_1)^{1/r} + t(x_1)^{1/r} + t(x_2)^{1/r})^r),$$

where r ($0 < r \leq 1$) is the dependence parameter. We can differentiate this w.r.t. z_1, x_1, x_2 to derive the density.

$$\begin{aligned}g(z_1, x_1, x_2) &= \frac{t(z_1)^{\xi_{z_1}+1}}{\sigma_{z_1}} \frac{t(x_1)^{\xi_{x_1}+1}}{\sigma_{x_1}} \frac{t(x_2)^{\xi_{x_2}+1}}{\sigma_{x_2}} t(z_1)^{\frac{1}{r}-1} t(x_1)^{\frac{1}{r}-1} t(x_2)^{\frac{1}{r}-1} \\ &\times \exp(-(t(z_1)^{1/r} + t(x_1)^{1/r} + t(x_2)^{1/r})^r) \\ &\times \left[\frac{(1-r)(2-r)}{r} - \left(\frac{1-r}{r} \right) (t(z_1)^{1/r} + t(x_1)^{1/r} + t(x_2)^{1/r})^r \right. \\ &\quad \left. + (t(z_1)^{1/r} + t(x_1)^{1/r} + t(x_2)^{1/r})^{2r} \right] \\ &\times (t(z_1)^{1/r} + t(x_1)^{1/r} + t(x_2)^{1/r})^{r-3}.\end{aligned}$$

Then the log-likelihood is given by,

$$\begin{aligned}
& l(\theta|Z_1, X_2, X_1; Z_2) \\
&= \sum_{i=1}^n \left((\xi_{z_1} + 1) \log(t(z_{1i})) - \log(\sigma_{z_1}) + (\xi_{x_1} + 1) \log(t(x_{1i})) - \log(\sigma_{x_1}) \right. \\
&\quad + (\xi_{x_2} + 1) \log(t(x_{2i})) - \log(\sigma_{x_2}) + \left. \left(\frac{1}{r} - 1 \right) \log(t(z_{1i})) \right. \\
&\quad + \left. \left(\frac{1}{r} - 1 \right) \log(t(x_{1i})) + \left(\frac{1}{r} - 1 \right) \log(t(x_{2i})) \right. \\
&\quad - (t(z_{1i})^{1/r} + t(x_{1i})^{1/r} + t(x_{2i})^{1/r})^r \\
&\quad + \log \left[\frac{(1-r)(2-r)}{r} \right. \\
&\quad - \left. \left(\frac{1-r}{r} \right) (t(z_{1i})^{1/r} + t(x_{1i})^{1/r} + t(x_{2i})^{1/r})^r \right. \\
&\quad \left. \left. + (t(z_{1i})^{1/r} + t(x_{1i})^{1/r} + t(x_{2i})^{1/r})^{2r} \right] \right. \\
&\quad \left. + (r-3) \log(t(z_{1i})^{1/r} + t(x_{1i})^{1/r} + t(x_{2i})^{1/r}) \right)
\end{aligned}$$

Priors:

$$\begin{aligned}
\alpha_0, \alpha_1, \beta_0, \beta_1, \beta_2 &\stackrel{iid}{\sim} N(0, 10^2) \\
\gamma_0, \gamma_1, \gamma_2, \gamma_3 &\stackrel{iid}{\sim} N(0, 10^3) \\
\sigma_{z_1}, \sigma_{x_1}, \sigma_{x_2} &\stackrel{iid}{\sim} \text{IG}(\alpha = 1, \beta = 1) \\
\xi_{z_1} &\sim \text{Unif}(-1, 1) \\
\xi_{x_1}, \xi_{x_2} &\stackrel{iid}{\sim} \text{Unif}(-0.5, 0.5) \\
r &\sim \text{Unif}(-0.05, 1)
\end{aligned}$$

The priors have been chosen based on well-known information about GEV models and keeping in the mind the frequentist univariate model estimates. The standard regularity conditions for the likelihood of an GEV are satisfied for $\xi < 0.5$. In particular for the range of values $-0.5 < \xi < 0.5$ are most often encountered in practice⁹⁰. Hence, we model the shape parameters by a uniform prior between -0.5 and 0.5. Since, in our parameterization of the dependence parameter, r , $0 < r \leq 1$, we model it using a Uniform distribution but with a lower bound of 0.05 to avoid computational overflow. Other priors are non-informative.

We have 16 unknown parameters in this model and the step-sizes for the Metropolis Hastings (MH) algorithm have been chosen such that the acceptance rate for the MH-algorithm is about 20%, which is the generally accepted as a good enough acceptance rate. Note that we also standardize X_1 to fit in the third model (as a covariate) as is recommended while fitting GEV models.

The Metropolis Hastings algorithm is run for 10^6 MCMC steps and we present the posterior means and standard deviations for the parameters in Table 5. We notice that while the estimates for the location parameters are close for the frequentist and the Bayesian models, the shape and scale parameter estimates vary. The shape parameter for Z_1 ($\log(\text{minCP})$) is -0.586 in the frequentist model while it is -0.434 for the Bayesian trivariate GEV model, which is within the consistency range for the MLE of the shape parameter, ξ . The shape parameter estimate for X_1 ($\log(\text{maxWS})$) decreases from -0.352 in the frequentist univariate case to -0.487 in the Bayesian trivariate case, while the estimate for X_2 ($\log(\text{damages})$) increases from -0.327 in the frequentist univariate case to -0.184 in the Bayesian trivariate case. Interestingly, the estimate for dependence parameter r is 0.997 which is very close to 1 signifying independence between the three variables considered. We suspect that this is because the non-stationarity considered in location parameters already accounts for the dependence between the three variables. The results seem pretty stable on change on starting values and modifications to the prior specifications.

The results of Table 5 are very close to those of Table 1, where we obtained the results using the hierarchical Bayesian GEV model. Thus, the conclusions from the data are quite robust to the data science framework used for analysis.

C.2 Individuation Cyclones: Hierarchical Model with Log-Normal Damage

Since it is possible that cyclone damages follow a heavy-tailed but not necessarily extreme valued distribution, we model it has a log-normal distribution in this section. The overall structure remains the same as Section 6. Note, Z_1 represents $\log(\text{minCP})$, Z_2 is for standardized average latitude, X_1 represents $\log(\text{maxWS})$ and X_2 is for damages. We consider the following model:

$$Z_1|Z_2 \sim \text{GEV}(\mu_{z_1}(Z_2), \sigma_{z_1}, \xi_{z_1}) \quad (45)$$

$$X_1|(Z_1, Z_2) \sim \text{GEV}(\mu_{x_1}(Z_1, Z_2), \sigma_{x_1}, \xi_{x_1}) \quad (46)$$

$$X_2|(X_1, Z_1, Z_2) \sim \text{Lognormal}(\mu_{x_2}(X_1, Z_1, Z_2), \sigma_{x_2}), \quad (47)$$

where the hierarchy essentially comes in the location parameters,

$$\begin{aligned} \mu_{z_1}(Z_2) &= \alpha_0 + \alpha_1 Z_2 \\ \mu_{x_1}(Z_1, Z_2) &= \beta_0 + \beta_1 Z_1 + \beta_2 Z_2 \\ \mu_{x_2}(X_1, Z_1, Z_2) &= \gamma_0 + \gamma_1 X_1 + \gamma_2 Z_1 + \gamma_3 Z_2. \end{aligned}$$

The joint density can then be written as,

$$\begin{aligned}
& f(Z_1, X_1, X_2|Z_2, \theta) \\
&= f(X_2|X_1, Z_1, Z_2)f(X_1|Z_1, Z_2)f(Z_1|Z_2) \\
&= \frac{1}{x_2\sigma_{x_2}\sqrt{2\pi}} \exp\left(-\frac{(\log(x_2) - \mu_{x_2}(x_1, z_1, z_2))^2}{2\sigma_{x_2}^2}\right) \\
&\quad \times \frac{1}{\sigma_{x_1}} (t(x_1))^{\xi_{x_1}+1} \exp(-t(x_1)) \\
&\quad \times \frac{1}{\sigma_{z_1}} (t(z_1))^{\xi_{z_1}+1} \exp(-t(z_1)),
\end{aligned}$$

where,

$$t(x) = \begin{cases} (1 + \xi(\frac{x-\mu}{\sigma}))^{-1/\xi} & \xi \neq 0 \\ \exp(-\frac{x-\mu}{\sigma}) & \xi = 0. \end{cases}$$

Then the log-likelihood can be given by,

$$\begin{aligned}
l(\theta|X_1, X_2, Z_1, Z_2) &= \sum_{i=1}^n \left[-\log(x_{2i}\sigma_{x_2}\sqrt{2\pi}) - \frac{(\log(x_{2i}) - \mu_{x_2})^2}{2\sigma_{x_2}^2} \right. \\
&\quad - \log(\sigma_{x_{1i}}) + (\xi_{x_{1i}} + 1) \log(t(x_{1i})) - t(x_{1i}) \\
&\quad \left. - \log(\sigma_{z_{1i}}) + (\xi_{z_{1i}} + 1) \log(t(z_{1i})) - t(z_{1i}) \right].
\end{aligned}$$

Priors: The location parameter priors for both the GEV models (minCP and maxWS) and the log-normal model (damages) are non-informative with variances chosen to be drawn for Inverse-Gamma(1,1) to ensure proper coverage of the sample space leading to good acceptance rates.

$$\begin{aligned}
\alpha_0, \alpha_1 &\stackrel{iid}{\sim} N(0, 10^3) \\
\beta_0, \beta_1, \beta_2 &\stackrel{iid}{\sim} N(0, 10^2) \\
\gamma_0, \gamma_1, \gamma_2, \gamma_3 &\stackrel{iid}{\sim} N(0, 10^3) \\
\sigma_{z_1}, \sigma_{x_1}, \sigma_{x_2} &\stackrel{iid}{\sim} \text{IG}(\alpha = 1, \beta = 1) \\
\xi_{z_1} &\sim \text{Unif}(-1, 1) \\
\xi_{x_1} &\stackrel{iid}{\sim} \text{Unif}(-0.5, 0.5).
\end{aligned}$$

We use Metropolis-Hastings algorithm to sample from the posterior distribution. The chain is run for $N = 10^6$ MCMC sample size and the step-sizes are chosen to achieve about 20% acceptance rate. The results from this model fitting is given in Table 6. The results of this are very close to those in Table 5 and Table 1, where we reported the results using the trivariate Bayesian GEV model and the hierarchical Bayesian GEV model respectively. Thus, the conclusions from the data are quite robust to the data science framework used for analysis.

Note that the frequentist estimates for the location parameters are similar to the posterior means for the location parameters. The shape and scale parameters differ, similar to how they differed in the trivariate GEV model of Section C.1 and Bayesian hierarchical GEV model in Section 6. In terms of significance of estimates, coefficient of average latitude (α_1) in modeling location parameter for minCP is statistically significant. Similarly, the effect of minCP (β_1) and average latitude (β_2) in modeling location parameter for maxWS seems to be significant. The standard errors for the coefficient estimates for damages are high, resulting in non-significant effect corresponding to maxWS, minCP and average latitude, on the location parameter of damages, with a highly significant intercept term. The scale parameter estimates are significant across models, and the first two models in the hierarchy have a negative estimate for the shape parameters signifying Reverse Weibull distributions for the marginals of each of $\log(\text{minCP})$ and $\log(\text{maxWS})$ respectively.

C.3 Individual Cyclones: Additional Predictions

Similar to the analysis presented in Section 3, we now present the prediction results for the Atlantic tropical cyclones of 2016-17 using the statistical models described in Section C.1 (trivariate Bayesian GEV) and in Section C.2 (hierarchical Bayesian model with log-Normal distribution for damages).

We consider the predictions from these models for the years 2016 and 2017. The details are same as those given in Section 3. We note from Table 7 that all the true minimum central pressure values were always within the 95% credible interval for all five cyclones. Even the true maximum wind speed fell within the intervals for all the three models, except it missed the mark very closely for hurricane Nate in hierarchical Bayesian model with log-Normal for damages. More specifically, the 95% credible interval for Nate was (3.1304, 4.3807) and the true value was 4.3820, on the log-scale. For damages, none of the credible intervals for the three models (hierarchical GEV in Section 3, trivariate GEV in Section C.1 and hierarchical model with log-Normal loss in Section C.2) could capture the observed value for Harvey in the 95% interval. However the damages due to Harvey is within the range of the posterior for the hierarchical GEV method of Section 3.

Similarly, the true damage value for Irma only fell in the 95% credible interval when the hierarchical GEV model of in Section 3 was fit, but was missed in the other two methods. However, the truth was not too far away in the tails of the predictive distribution. Given that Harvey and Irma both are in the top-five most damage causing Atlantic cyclones, these results are not surprising. We present the δ -values using the models described in Section C.1 and in Section C.2 in Tables 8 and 9 respectively. These values are not substantially different from those of Table 2.

D Appendix: All Tables

Table 3: Comparison of different statistical methodologies for analyzing the low intensity tropical cyclones data. Here, *all* refers to the model where all the covariates were used, while *selected* refers to where a few selected covariates were used. These were selected using a model selection criterion on a model with all covariates. The abbreviation EB refers empirical Bayes approach, while HB refers to hierarchical Bayesian approach that we use in the paper. The MCMC and dclone are two different computational approaches, the latter is non-Bayesian, but may be used in conjunction with empirical or hierarchical Bayesian techniques as well. Each entry is an expected value, with standard deviation in brackets. Results show excellent robustness across statistical methodologies.

Parameter	Method	All		Selected	
		EB	HB	EB	HB
β_{11} (NAO)	MCMC	-0.068 (0.059)	-0.068 (0.059)	-0.060 (0.059)	-0.060 (0.059)
	dclone	-0.068 (0.026)	-0.068 (0.026)	-0.060 (0.026)	-0.060 (0.026)
β_{12} (SOI)	MCMC	-0.016 (0.031)	-0.016 (0.031)	-	-
	dclone	-0.016 (0.014)	-0.016 (0.014)	-	-
β_{13} (AMO)	MCMC	-0.429 (0.211)	-0.429 (0.211)	-0.456 (0.208)	-0.456 (0.208)
	dclone	-0.429(0.092)	-0.429 (0.092)	-0.456 (0.092)	-0.456 (0.092)
β_{14} Nino-3.4	MCMC	-0.253 (0.103)	-0.254 (0.102)	-0.207 (0.075)	-0.207 (0.075)
	dclone	-0.253 (0.045)	-0.253 (0.045)	-0.207 (0.033)	-0.207 (0.033)
β_{15} (SST)	MCMC	0.098 (0.003)	0.098 (0.003)	0.100 (0.002)	0.100 (0.002)
	dclone	0.098 (0.001)	0.098 (0.001)	0.100 (0.001)	0.100 (0.001)
β_{16} (Sunspots)	MCMC	0.001 (0.001)	0.001 (0.001)	-	-
	dclone	0.001 (0.000)	0.001 (0.000)	-	-
r	MCMC	36.087 (15.590)	36.065 (15.540)	36.730 (15.474)	36.807 (15.512)
	dclone	37.118(11.046)	37.133 (11.064)	34.932 (10.447)	34.934 (10.439)
θ_1	MCMC	0.142 (0.011)	0.142 (0.011)	0.142 (0.011)	0.142 (0.011)
	dclone	0.142 (0.005)	0.142 (0.005)	0.142 (0.005)	0.142 (0.005)
μ_1	MCMC	18.297 (0.344)	18.296 (0.337)	18.295 (0.344)	18.296 (0.337)
	dclone	18.296 (0.149)	18.295 (0.149)	18.296 (0.149)	18.296 (0.149)
σ_1^2	MCMC	5.074 (1.155)	4.882 (1.091)	5.077(1.161)	4.884 (1.093)
	dclone	4.790 (0.467)	4.756 (0.461)	4.789 (0.466)	4.756 (0.463)

Table 4: Comparison of different statistical methodologies for analyzing the high intensity tropical cyclones data. Here, *all* refers to the model where all the covariates were used, while *selected* refers to where a few selected covariates were used. These were selected using a model selection criterion on a model with all covariates. The abbreviation EB refers empirical Bayes approach, while HB refers to hierarchical Bayesian approach that we use in the paper. The MCMC and dclone are two different computational approaches, the latter is non-Bayesian, but may be used in conjunction with empirical or hierarchical Bayesian techniques as well. Each entry is an expected value, with standard deviation in brackets. Results show excellent robustness across statistical methodologies.

Parameter	Method	All		Selected	
		EB	HB	EB	HB
β_{21} (NAO)	MCMC	0.140 (0.118)	0.140(0.118)	-	-
	dclone	0.137(0.053)	0.137 (0.053)	-	-
β_{22} (SOI)	MCMC	0.025 (0.061)	0.025 (0.061)	-	-
	dclone	0.024 (0.027)	0.024 (0.027)	-	-
β_{23} (AMO)	MCMC	1.908 (0.434)	1.907 (0.435)	1.738 (0.385)	1.740 (0.386)
	dclone	1.893 (0.193)	1.893 (0.194)	1.733 (0.172)	1.732 (0.173)
β_{24} Nino-3.4	MCMC	-0.223 (0.191)	-0.224 (0.191)	-0.321 (0.147)	-0.321 (0.147)
	dclone	-0.224 (0.085)	-0.224 (0.085)	-0.321 (0.066)	-0.321 (0.066)
β_{25} (SST)	MCMC	0.033 (0.006)	0.033 (0.006)	0.031 (0.004)	0.031 (0.004)
	dclone	0.034 (0.003)	0.034 (0.003)	0.031 (0.002)	0.031 (0.002)
β_{26} (Sunspots)	MCMC	-0.001(0.001)	-0.001(0.001)	-	-
	dclone	-0.001(0.001)	-0.001(0.001)	-	-
θ_2	MCMC	0.390(0.040)	0.391(0.040)	0.390 (0.040)	0.391(0.040)
	dclone	0.389 (0.018)	0.390 (0.018)	0.389 (0.018)	0.390 (0.018)
μ_2	MCMC	21.121 (0.447)	21.122(0.436)	21.120 (0.448)	21.121(0.435)
	dclone	21.121 (0.193)	21.121 (0.192)	21.121(0.193)	21.121 (0.192)
σ_2^2	MCMC	6.997 (1.794)	6.644(1.662)	6.993(1.798)	6.649(1.668)
	dclone	6.508 (0.705)	6.445(0.695)	6.510(0.705)	6.447 (0.695)

	Estimate	Std. Error	Posterior mean	Posterior SD
α_0	-0.1919	0.0930	-0.1048	0.0842
α_1	-0.2623	0.0608	-0.2723	0.0494
σ_{z_1}	1.0395	0.0744	0.7721	0.0302
ξ_{z_1}	-0.5859	0.0499	-0.4335	0.0407
β_0	4.3691	0.0128	4.2243	0.0305
β_1	0.3430	0.0151	0.3508	0.0282
β_2	-0.0449	0.0128	-0.0434	0.0305
σ_{x_1}	0.1429	0.0088	0.3549	0.0169
ξ_{x_1}	-0.3521	0.0444	-0.4875	0.0129
γ_0	19.5008	0.2033	19.2190	0.1730
γ_1	0.9391	0.5735	1.0601	0.3632
γ_2	0.5070	0.5535	0.4400	0.3497
γ_3	-0.1918	0.2068	-0.1338	0.1310
σ_{x_2}	2.2626	0.1394	1.5064	0.0562
ξ_{x_2}	-0.3275	0.0373	-0.1844	0.0246
r			0.9970	0.0039

Table 5: Frequentist estimates from models (45), (46), (47), and posterior mean and standard deviation from the trivariate Bayesian extreme value distribution (GEV) model

	Post means	Posterior sd	Frequentist est	Freq se
α_0	-0.1070	0.0859	-0.1919	0.0930
α_1	-0.2720	0.0499	-0.2623	0.0608
σ_{z1}	0.7724	0.0302	1.0395	0.0744
ξ_{z1}	-0.4330	0.0419	-0.5859	0.0499
β_0	4.2232	0.0308	4.3691	0.0128
β_1	0.3526	0.0283	0.3430	0.0151
β_2	-0.0426	0.0301	-0.0449	0.0128
σ_{x1}	0.3554	0.0171	0.1429	0.0088
ξ_{x1}	-0.4875	0.0128	-0.3521	0.0444
γ_0	20.1867	0.1196	20.2294	0.1831
γ_1	0.8188	0.3641	0.8162	0.5583
γ_2	0.7523	0.3531	0.7559	0.5422
γ_3	-0.2522	0.1316	-0.2545	0.2012
σ_{x2}	1.4364	0.0526	-	-

Table 6: Frequentist estimates from models (45), (46), (47), and posterior mean and standard deviation from the hierarchical Bayesian model with log-Normal damages

	minCP	maxWS	damages
Hierarchical GEV	100% (5/5)	100% (5/5)	80% (4/5)
Trivariate GEV	100% (5/5)	100 % (5/5)	60% (3/5)
Hierarchical log-Normal damages	100% (5/5)	80% (4/5)	60% (3/5)

Table 7: The proportion of cyclones in 2016-17 where the truth was contained in the 95% credible interval.

Hurricanes	minCP	maxWS	Damage
Hermine (2016)	0.8440	0.5432	0.3293
Matthew (2016)	0.3683	0.2023	0.1667
Harvey (2017)	0.2969	0.3514	0.0006
Irma (2017)	0.1964	0.1638	0.0430
Nate (2017)	0.9263	0.0516	0.4689

Table 8: For the hierarchical GEV model in Section C.1, δ values for each of the hurricanes, closer to 1 reflects the truth to be close to the median of the posterior predictive distribution and closer to 0 reflects the truth lying in the tails of the distribution.

Hurricanes	minCP	maxWS	Damage
Hermine (2016)	0.8256	0.5392	0.3424
Matthew (2016)	0.3823	0.2019	0.2104
Harvey (2017)	0.3038	0.3525	2e-04
Irma (2017)	0.2009	0.1656	0.0355
Nate (2017)	0.9159	0.0491	0.4783

Table 9: For the hierarchical GEV model with log-Normal damages in Section C.2, δ values for each of the hurricanes, closer to 1 reflects the truth to be close to the median of the posterior predictive distribution and closer to 0 reflects the truth lying in the tails of the distribution.

E Appendix:All Figures

Figure 5: Posterior predictive distributions for 2016 low intensity cyclones. The top row is for empirical Bayes prediction, the middle row is for fast Bayesian prediction and the bottom row is for hierarchical Bayesian prediction. The left column is the probability mass function for cyclone frequency, middle column is for damage-inflicting probability, and right column is density for logarithm of damages. The actual values are displayed with red dashed lines.

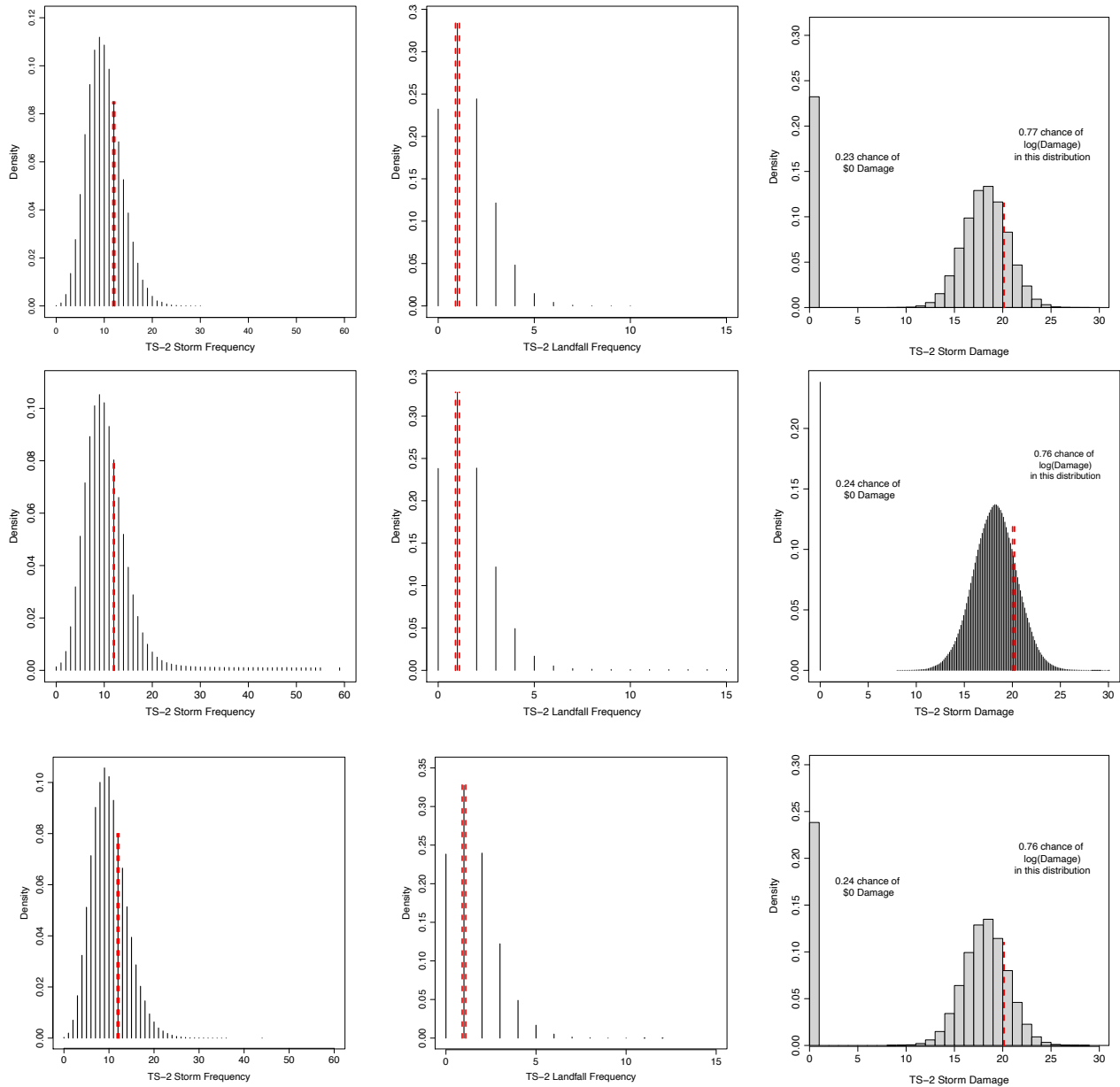


Figure 6: Posterior Predictive Distributions for 2016 High Intensity cyclones. The top row is for empirical Bayes prediction, the middle row is for fast Bayesian prediction and the bottom row is for hierarchical Bayesian prediction. The left column is the probability mass function for cyclone frequency, middle column is for damage-inflicting probability, and right column is density for logarithm of damages. The actual values are displayed with red dashed lines.

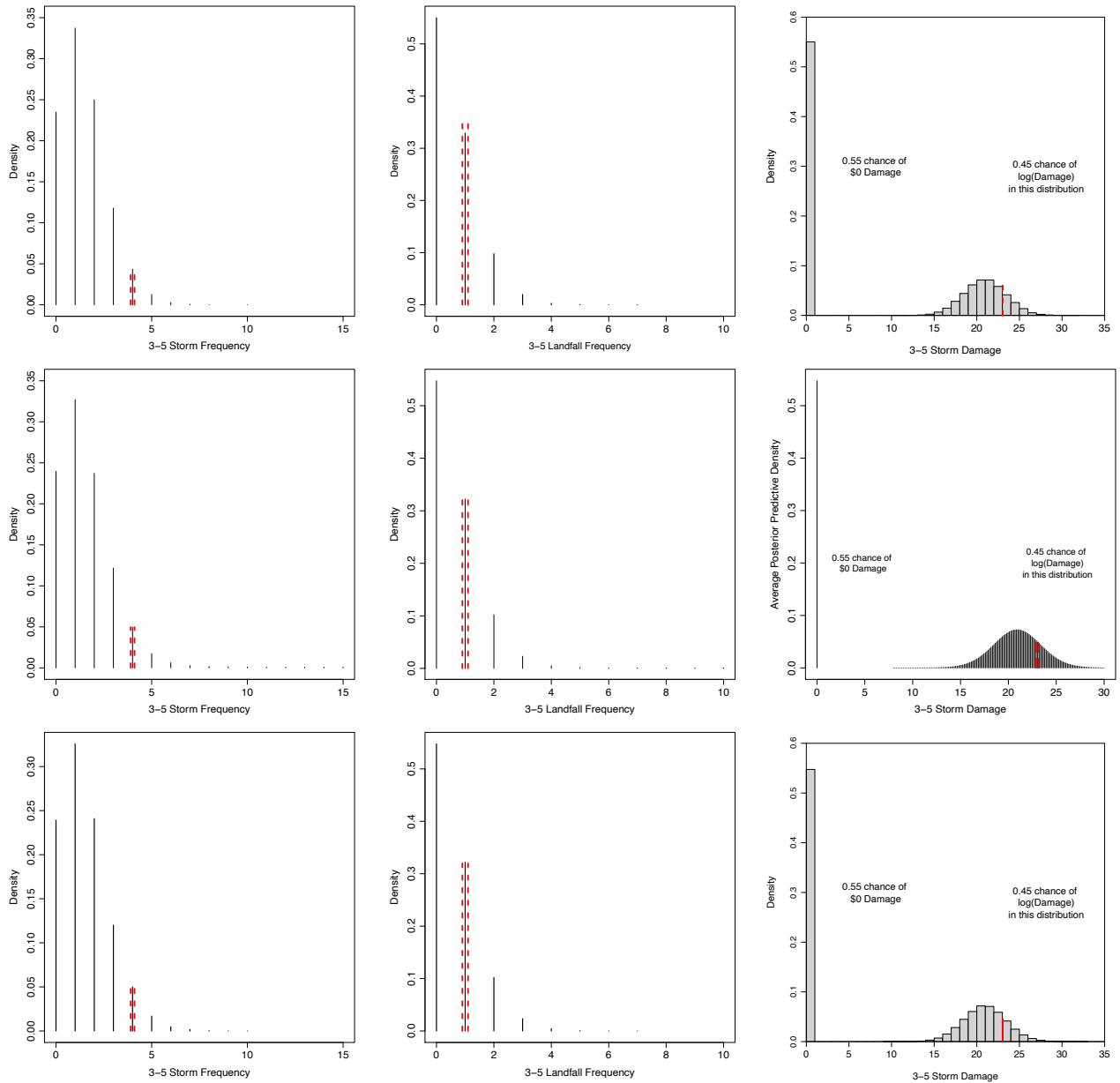


Figure 7: Posterior Predictive Distributions for 2017 Low Intensity cyclones. The top row is for empirical Bayes prediction, the middle row is for fast Bayesian prediction and the bottom row is for hierarchical Bayesian prediction. The left column is the probability mass function for cyclone frequency, middle column is for damage-inflicting probability, and right column is density for logarithm of damages. The actual values are displayed with red dashed lines.

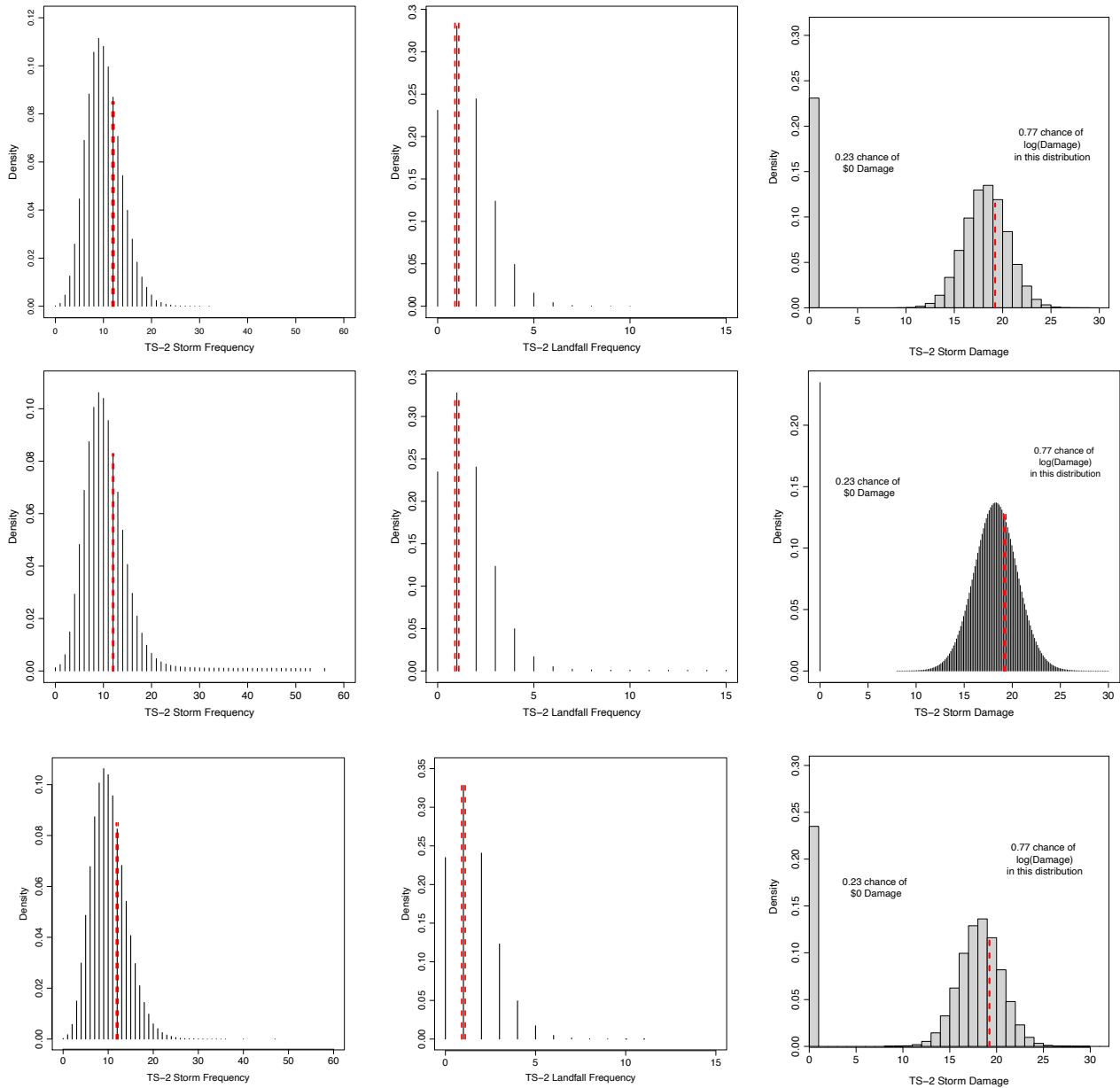


Figure 8: Posterior Predictive Distributions for 2017 High Intensity cyclones. The top row is for empirical Bayes prediction, the middle row is for fast Bayesian prediction and the bottom row is for hierarchical Bayesian prediction. The left column is the probability mass function for cyclone frequency, middle column is for damage-inflicting probability, and right column is density for logarithm of damages. The actual values are displayed with red dashed lines.

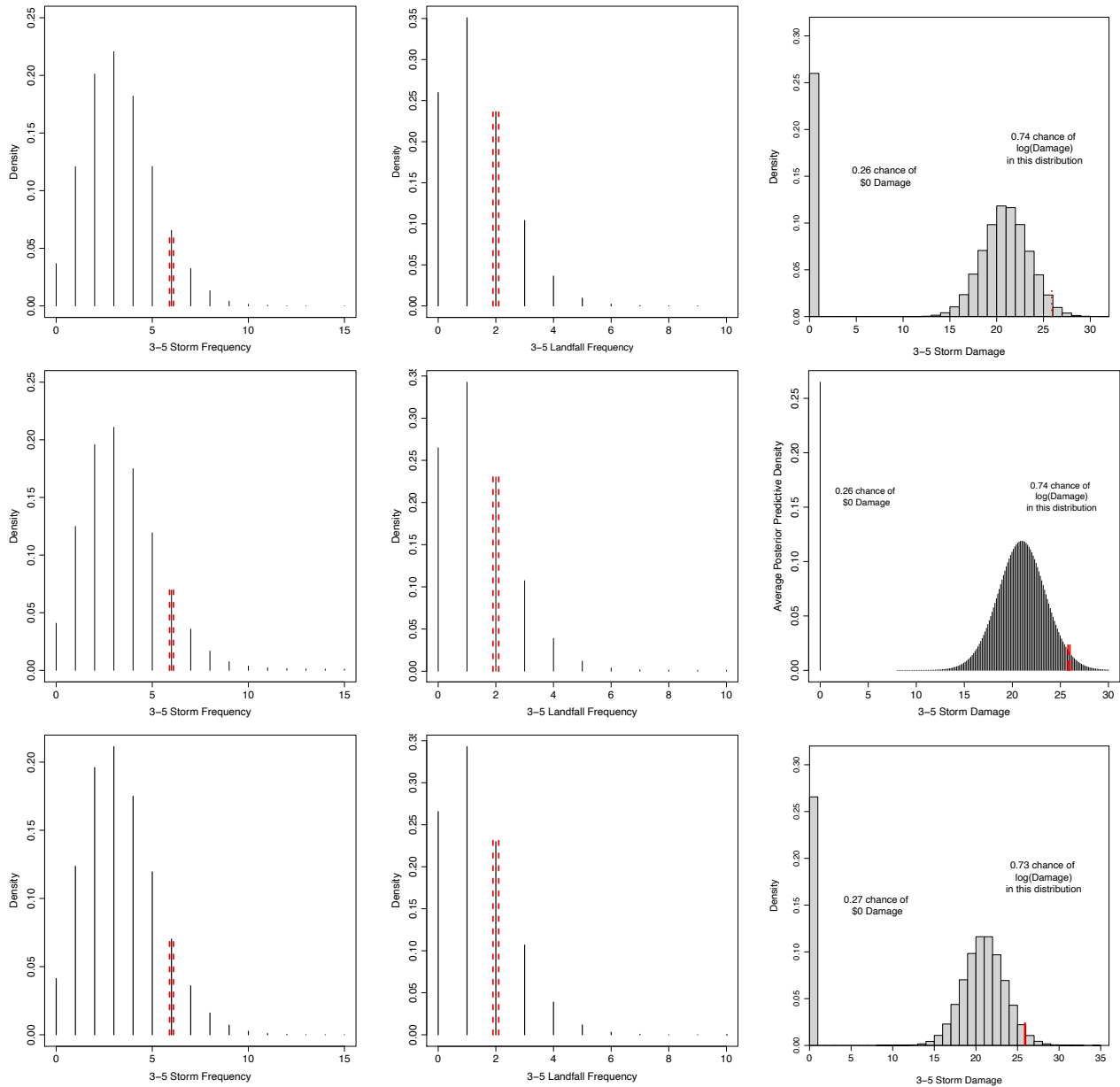


Figure 9: Posterior Predictive Distributions for 2018 Low Intensity cyclones. The top row is for empirical Bayes prediction, the middle row is for fast Bayesian prediction and the bottom row is for hierarchical Bayesian prediction. The left column is the probability mass function for cyclone frequency, middle column is for damage-inflicting probability, and right column is density for logarithm of damages. The actual values are displayed with red dashed lines.

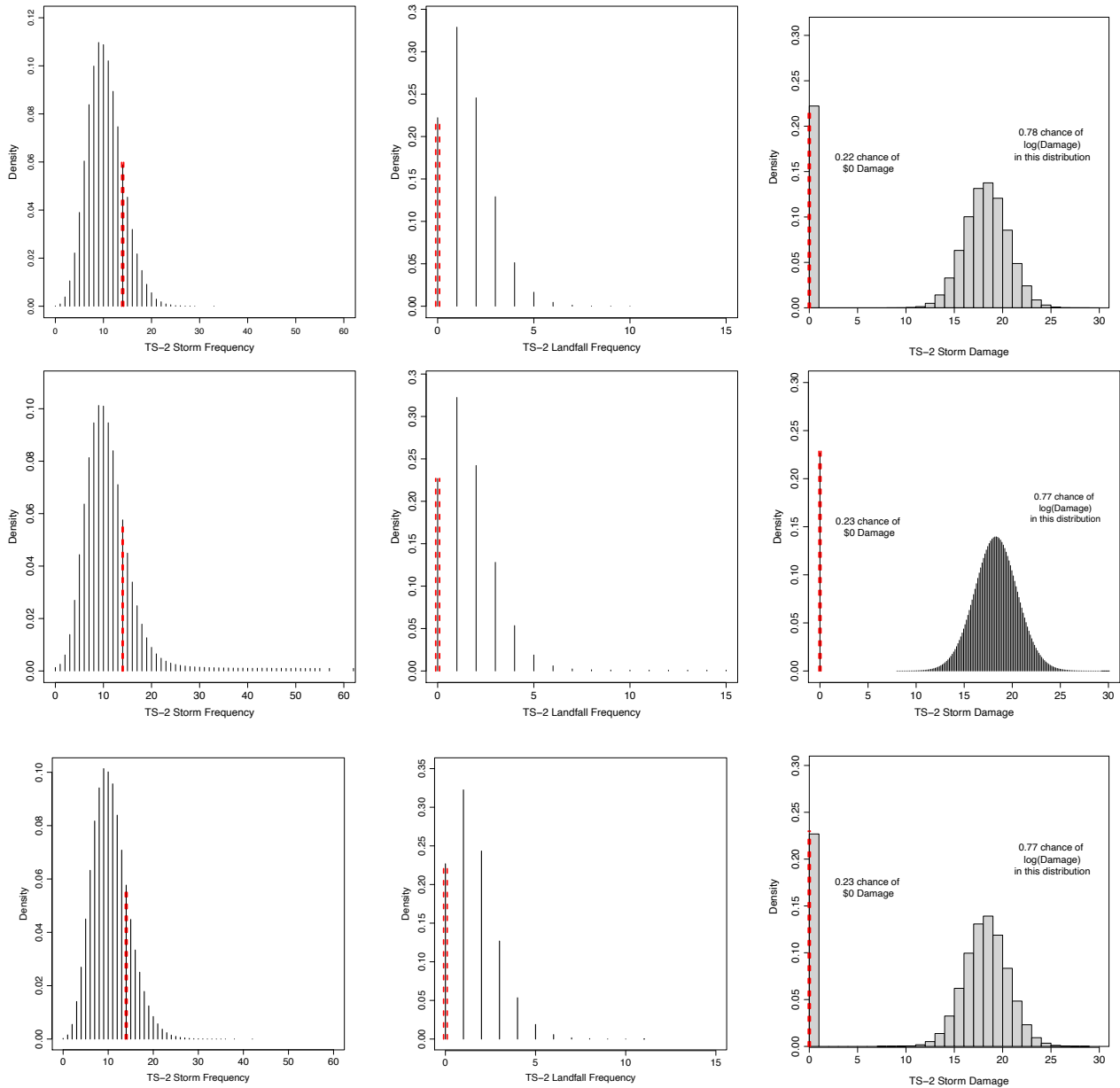


Figure 10: Posterior Predictive Distributions for 2018 High Intensity cyclones. The top row is for empirical Bayes prediction, the middle row is for fast Bayesian prediction and the bottom row is for hierarchical Bayesian prediction. The left column is the probability mass function for cyclone frequency, middle column is for damage-inflicting probability, and right column is density for logarithm of damages. The actual values are displayed with red dashed lines.

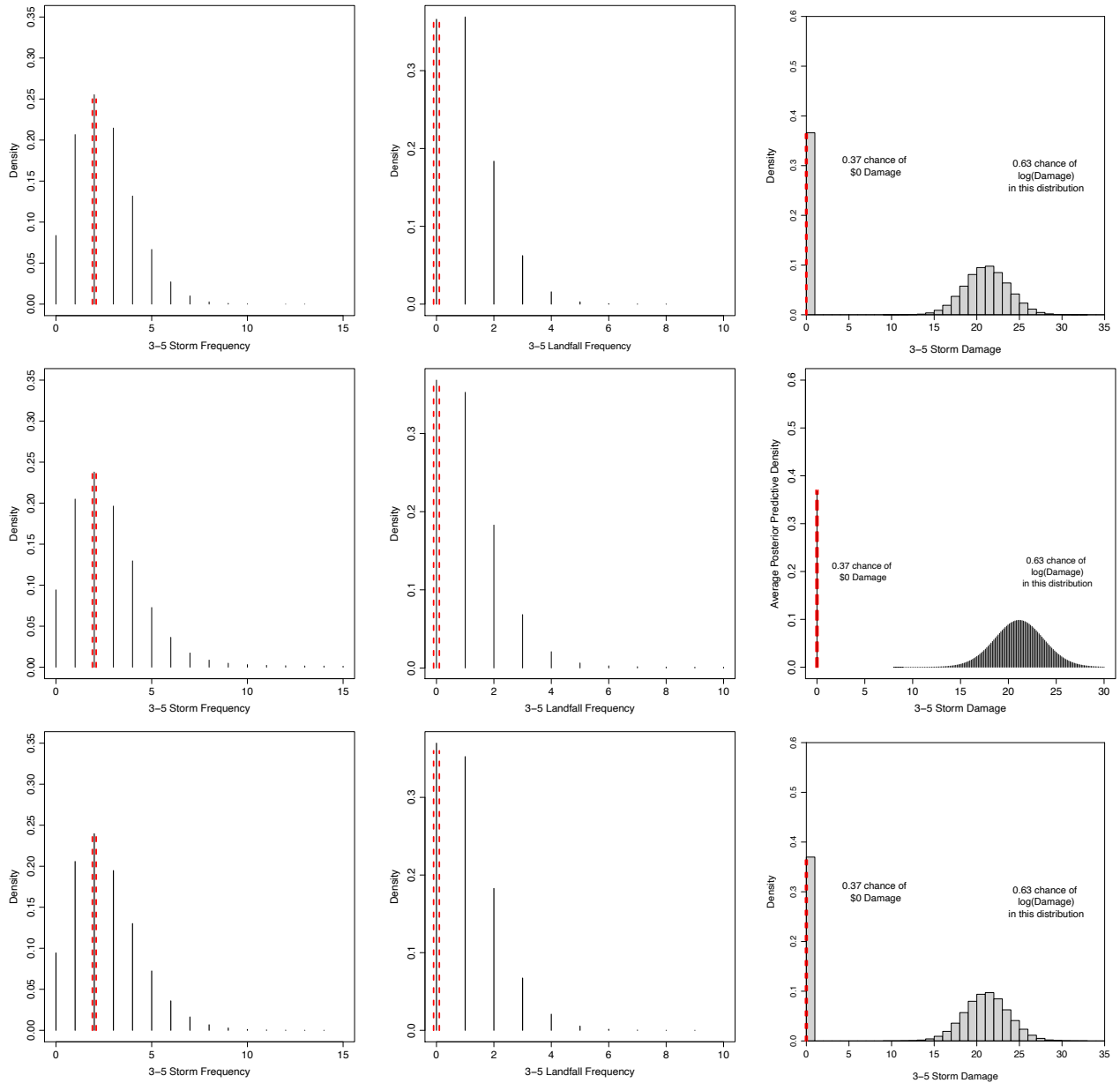


Figure 11: Posterior Predictive Distributions for 2019 Low Intensity cyclones. The top row is for empirical Bayes prediction, the middle row is for fast Bayesian prediction and the bottom row is for hierarchical Bayesian prediction. The left column is the probability mass function for cyclone frequency, middle column is for damage-inflicting probability, and right column is density for logarithm of damages. The actual values are displayed with red dashed lines.

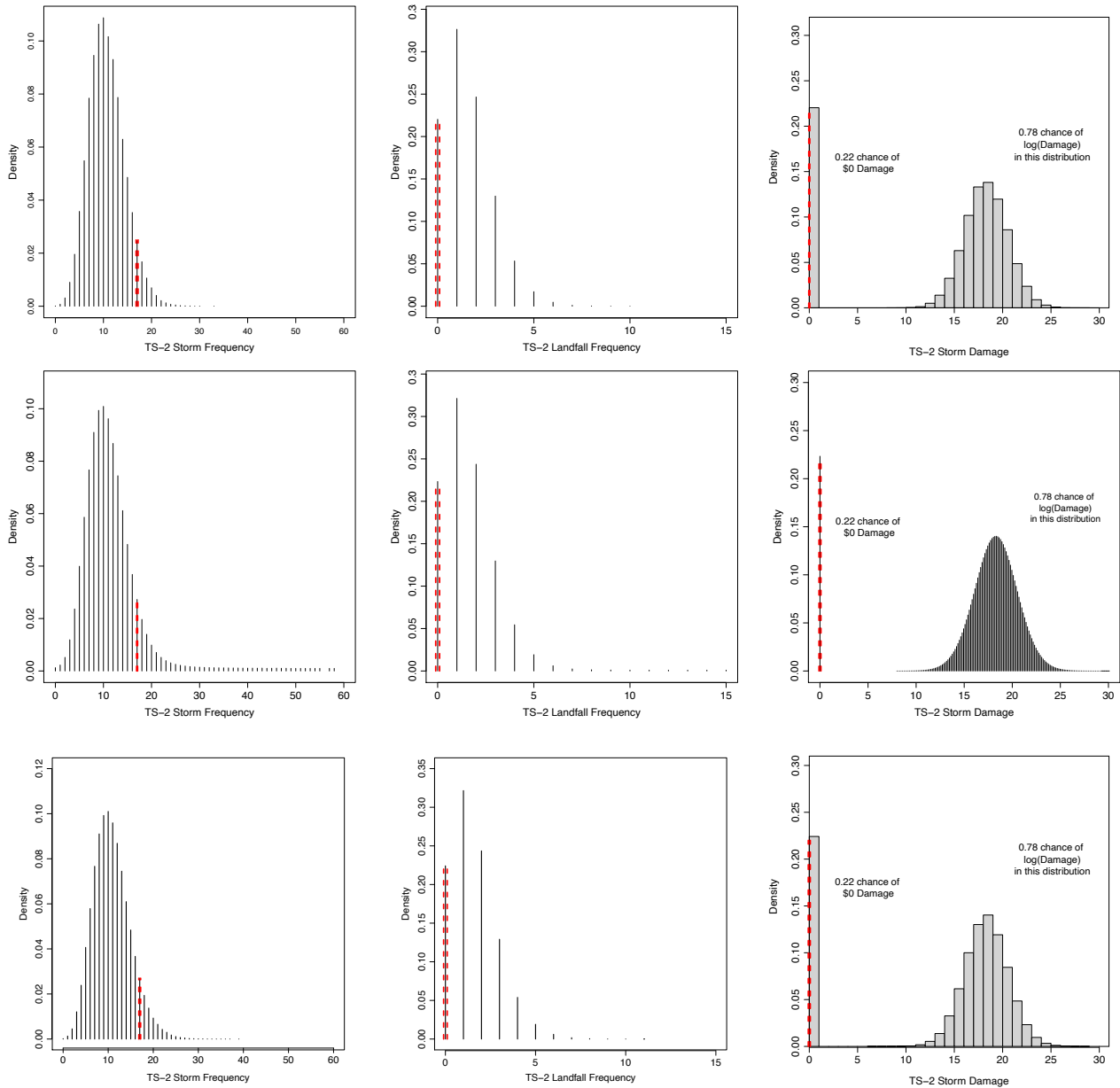


Figure 12: Posterior Predictive Distributions for 2019 High Intensity cyclones. The top row is for empirical Bayes prediction, the middle row is for fast Bayesian prediction and the bottom row is for hierarchical Bayesian prediction. The left column is the probability mass function for cyclone frequency, middle column is for damage-inflicting probability, and right column is density for logarithm of damages. The actual values are displayed with red dashed lines.

